

Corrosion of Alternative Grades of Reinforcing Steel in Concrete

**by
Md A. Islam**

**A thesis
presented to the University of Waterloo
in fulfilment of the
thesis requirement for the degree of
Master of Applied Science
in
Mechanical Engineering**

**Waterloo, Ontario, Canada, 2010
© Md A. Islam 2010**

Author's Declaration

I hereby declare that I am the sole author of this thesis. This is a true copy of the thesis, including any required final revisions, as accepted by my examiners.

I understand that my thesis may be made electronically available to the public.

Md A. Islam

Abstract

Reinforcing steel in concrete has been used for many years in roads, bridges and other structures to give strength and durability; concrete has only good compressive strength and reinforcing steel gives the tensile strength to the concrete to sustain both the compressive and tensile load, making concrete structures to be used in the common as well as critical areas. Reinforcing steel that was used in structures predominantly is mild steel, which is considerably cheaper than stainless steel, and more susceptible to corrosion leading to the damage of the structures and less longevity.

To solve the problem with the use of mild steel in critical areas, such as bridges; stainless steel is used; which has iron as the main constituents along with the chromium as the major alloying element and various grades are manufactured varying the compositions of steel. To reduce the cost of the stainless steel, some compositions like chromium, molybdenum, nickel are varied; especially the nickel is being replaced by manganese, the cost of which is significantly less than that of nickel.

The alternative grades of the reinforcing steel that were used for testing the corrosion resistance are mild steel (400), weldable mild steel (400 W) and four stainless steel 316LN, UNS 24100 (Enduramet 32), 2304, LDX 2101; among them 316LN and UNS 24100 are the austenitic steels (Valbruna) and 2304 and LDX 2101 are duplex steels (Outokumpu). The austenitic steels have no ferritic phase which is making austenitic steel more corrosion resistance than the duplex steels which have almost equal parts of the ferritic and austenitic phases.

Concrete that is used commonly as the shield for the reinforcing steel providing the environment to passivate the reinforcement. Concrete has the pH of ~13.5 which is the equivalent to the pH of the pore solution. Its strength and curing time varies due to the water cement ratio and composition and also the environment in which it is placed. Good quality concrete has less permeability and fewer cracks thereby limiting the ingress of the de-icing slats to the reinforcing steel and delaying the onset of corrosion.

Corrosion of the reinforcing steels was tested in concrete using both an accelerated exposure test and ASTM A 955M standard for cracked prisms to measure the corrosion rate and open circuit potential, which are quantitative measurement for corrosion. It is hoped that the results will provide a guide for the future use of the alternative grades of the reinforcing steel to be used in the concrete. Reinforcing mild steels were compared to determine if there is any advantage in using the more carefully controlled 400W welding grade, rather than the 400 grade. The service life of structures with the 400 grade of steel is well established and so the data from the 400 grade also provided a relative measure of corrosion resistance for the alternative grades of the stainless steel.

Microcell corrosion of the reinforcing steel was monitored by the use of the linear polarization and the corrosion potential. The data for show that there is no significant corrosion on any of the stainless steels after 15 months of measurement, whereas both the mild steels embedded in the concrete corroded fully as confirmed by visual observation of the beams after autopsying. The autopsied samples were then analysed for chloride content in the concrete adjacent to the reinforcing bars. This was accomplished by titration. The chloride content on the beams with 400 and 400W grades was found to be higher than the beams with the stainless steels, where the percentage of chloride remained almost the same.

Macrocell corrosion tests were performed on the ASTM A 955M cracked prisms and showed changes in corrosion current density in agreement with the accelerated corrosion current density of the stainless steels. The only difference was observed in the corrosion potentials of the 400 and 400W steels, which were more negative in the cracked prisms than in the beams.

In summary, all the stainless steels showed evident corrosion resistance both in accelerated and ASTM A 955M prisms tests and no sign of corrosion was found in the stainless steels after 400 days in beams and 200 days in prisms. The regular and weldable steels corroded in both tests in agreement with the data present in research.

Acknowledgements

I would like to thank my supervisor Dr. Carolyn Hansson for her kind assistance and guidance to carry out the research. I have learned immense that I cannot tell in words. She was the best guardian that I could have in this Canadian environment.

I would like to thank my all colleagues Dr. Shahzama Jaffer, Aditya Chattopadhyay, Brad Bergsma, Kyle Anders, Neal Damgaard, Heather Austin for their kind assistance and help that one could expect from colleagues. It's been really great to work with co-op students Matt Hunt, Khashayar Toutounchian, Jennifer Won, Cecilia Hou and Tom Coichon.

Thanks to Norval Wilhelm, Richard Morrison, Jorge A. Cruz, Doug Hrist, Ken Bowmen, Kwai Chan, John Bolt, Rob Kraemer, Rob Lepage, Robert Kaptein, Juan Ulloa, Neil Griffett, Fred Bakker, and Tom Gawel from different labs. Without their physical support, I would not have finished all the casting of my specimens.

I am grateful to Dr. Tom Ruttan and Kristine Meier for helping me to cope with the study and supporting me dealing with the critical situations in my life. I also want to thank Dr. Fue-Sang Lien, Dr. Richard Culham, Dr. John Medley, Dr. Pearl Sullivan, Dr. Mustafa Yavuz, Dr. Jeff West, and Nancy Oczkowski.

Special thanks to Mr. Frank Pianca from the Ministry of Transportation, Ontario (MTO) for funding the project which helped me to carry out my study and broadening my learning and to Valbruna Canada and Outokumpu for providing the steels and to Dufferin Concrete for supplying the concrete.

I would like to thank Dr. Mary Wells and Dr. Kaan Inal, the members of the review committee for my MASc thesis with their helpful comments, assistance and guidance. Above all, I am grateful to the Almighty and my family for their lifelong care and support to continue my study.

Table of Contents

List of Figures.....	viii
List of Tables.....	xi
1 Introduction	1
1.1 Reinforcing steels used for testing	3
2 Literature review	5
2.1 Reinforced concrete:.....	5
2.2 Properties of concrete	6
2.3 Reinforcing steels	7
2.3.i <i>Benefits of using reinforcing steel</i>	8
2.4 Corrosion of reinforcing steel.....	8
2.4.i <i>Effect of chloride on reinforcing steel</i>	11
2.4.ii <i>Reinforcing steel electrochemistry</i>	12
2.5 Effect of corrosion products on the reinforcing steel	14
2.5.i <i>Reduction in strength</i>	14
2.5.ii <i>Prevention of the corrosion</i>	15
2.6 Concrete degradation and its effects.....	17
2.6.i <i>Effect of chloride on concrete</i>	18
2.6.ii <i>Cracking of the concrete</i>	19
2.7 Microcell and Macrocell corrosion:	20
2.8 Concluding remarks.....	22
3 Experimental procedure	23
3.1 Types of reinforcing steels:	23
3.2 Accelerated testing of the reinforcing steel	24
3.2.i <i>Design of the test beams</i>	26
3.2.ii <i>Preparation of the test specimens</i>	28
3.2.iii <i>Casting of the concrete</i>	29
3.2.iv <i>Accelerated corrosion test setup and corrosion measurement of the reinforcing steel</i>	30
3.2.v <i>Electrochemical techniques used for the testing of steel</i>	32
3.3 Macrocell monitoring of the reinforcing steel in cracked concrete.....	33

3.3.i	<i>Design used for testing</i>	33
3.3.ii	<i>Preparation of the test materials</i>	34
3.3.iii	<i>Casting of the materials</i>	35
3.3.iv	<i>Macrocell corrosion setup and measurement</i>	36
3.3.v	<i>Electrochemical techniques used for the measurement</i>	38
4	Experimental results and discussion	39
4.1	Corrosion of the reinforcing steel under accelerated test	39
4.1.i	<i>Microcell corrosion</i>	39
4.1.ii	<i>Corrosion potential</i>	42
4.1.iii	<i>Visual inspection of the reinforcement for the beams</i>	45
4.2	Macrocell corrosion of the reinforcing steel under accelerated test	48
4.2.i	<i>Macrocell corrosion</i>	48
4.2.ii	<i>Corrosion potential</i>	51
4.2.iii	<i>Microstructure of the steels</i>	56
4.2.iv	<i>Chloride analysis of the concrete of the beams</i>	57
5	Summary, Conclusions and Recommendations	59
	References	61
	Appendix A Drill bits and Taps	69
	Appendix B Reference Electrodes	70
	Appendix C Titanium Mesh	71
	Appendix D Concrete Composition	72
	Appendix E Actual composition of the rebar	73

List of Figures

Figure 1: Variation of (A) the corrosion potential and (B) the corrosion current density of the reinforcing steel as a function of time for the specimen immersed in a 3.5 % NaCl solution (Rong-Gui Du et al., 2006).....	2
Figure 2: Different types of steels under investigation	3
Figure 3: Failure surface in the case of pull-out failure of (a) a ribbed bar and (b) a smooth bar (K. Lundgren, 2007)	5
Figure 4: Schematic illustration of the corrosion of steel reinforcement in concrete – as an electrochemical process (Shamsad, 2003).....	9
Figure 5: Steel corrosion process and current flow in concrete (J. Zhang et al., 2006) .	16
Figure 6: Chloride induced reinforcement corrosion process (D. Chen et al., 2008).....	18
Figure 7: Schematic illustration of microcell corrosion (C. M. Hansson et al., 2006)...	20
Figure 8: Schematic illustration of macrocell corrosion (C. M. Hansson et al., 2006)..	20
Figure 9: Schematic microcell and macrocell corrosion of the active steel (J. Zhang et al., 2006).....	21
Figure 10: Schematic microcell and macrocell corrosion of the passive steel (J. Zhang et al., 2006).....	22
Figure 11: Final accelerated corrosion measurement design for the beams.....	27
Figure 12: One of the six beams under investigation	27
Figure 13: Formwork made for the beams	29
Figure 14: Compressive strength of the cylinders casted for the beams	30
Figure 15: Schematic accelerated corrosion test setup and wiring diagram.....	30
Figure 16: Linear polarization resistance principle	32
Figure 17: Schematic illustration of the specimen design (ASTM A 955M).....	33
Figure 18: Picture of the shim used for casting of the prisms	34
Figure 19: Form work for the casting of the ASTM A 955M prisms	35
Figure 20: Top surface of the actual prism after the coating.....	36
Figure 21: Schematic setup of the ASTM A 955M prism.....	36
Figure 22: Actual picture of the cracked prism with the setup.....	37
Figure 23: Microcell corrosion current density for 316 LN rebar in beams	39

Figure 24: Microcell corrosion current density for UNS 24100 rebar in beams	39
Figure 25: Microcell corrosion current density for 2304 rebar in beams	40
Figure 26: Microcell corrosion current density for LDX 2101 rebar in beams.....	40
Figure 27: Microcell corrosion current density for 400 W rebar in beams	41
Figure 28: Microcell corrosion current density for 400 rebar in beams.....	41
Figure 29: Corrosion potential for 316 LN bars in beams.....	42
Figure 30: Corrosion potential for UNS 24100 bars in beams	42
Figure 31: Corrosion potential for 2304 bars in beams	43
Figure 32: Corrosion potential for LDX 2101 bars in beams.....	43
Figure 33: Corrosion potential for 400 W bars in beams	44
Figure 34: Corrosion potential for 400 bars in beams	44
Figure 35: Surface of 316 LN bars after breaking open three bars from the beams	45
Figure 36: Surface of UNS 24100 bars after breaking open three bars from the beams	45
Figure 37: Surface of 2304 bars after breaking open three bars from the beams.....	46
Figure 38: Surface of LDX 2101 bars after breaking open three bars from the beams .	46
Figure 39: Surface of 400 W bars after breaking open three bars from the beams	47
Figure 40: Surface of 400 bars after breaking open three bars from the beams.....	47
Figure 41: Macrocell corrosion current density for 316 LN rebar in prisms	48
Figure 42: Macrocell corrosion current density for UNS 24100 rebar in prisms.....	48
Figure 43: Macrocell corrosion current density for UNS 24100 rebar 4 in prisms.....	49
Figure 44: Macrocell corrosion current density for 2304 rebar in prisms.....	49
Figure 45: Macrocell corrosion current density for LDX 2101 rebar in prisms	50
Figure 46: Macrocell corrosion current density for 400 W rebar in prisms.....	50
Figure 47: Macrocell corrosion current density for 400 rebar in prisms.....	51
Figure 48: Corrosion potential for 316 LN top bars in prisms	51
Figure 49: Corrosion potential for UNS 24100 top bars in prisms	52
Figure 50: Corrosion potential for 2304 top bars in prisms	52
Figure 51: Corrosion potential for LDX 210 top bars in prisms	52
Figure 52: Corrosion potential for 400 W top bars in prisms.....	53
Figure 53: Corrosion potential for 400 top bars in prisms	53
Figure 54: Corrosion potential for 316 LN bottom bars in prisms.....	54

Figure 55: Corrosion potential for UNS 24100 bottom bars in prisms	54
Figure 56: Corrosion potential for 2304 bottom bars in prisms	54
Figure 57: Corrosion potential for LDX 2101 bottom bars in prisms	55
Figure 58: Corrosion potential for 400 W bottom bars in prisms	55
Figure 59: Corrosion potential for 400 bottom bars in prisms	55
Figure 60: Microstructure of the 316 LN rebar	56
Figure 61: Microstructure of the UNS 24100 rebar	56
Figure 62: Microstructure of 2304 rebar	56
Figure 63: Microstructure of LDX 2101 rebar	56
Figure 64: Microstructure of the 400 W rebar.....	57
Figure 65: Microstructure of the 400 top and bottom rebar	57
Figure 66: Weight percentage of chloride in concrete for the beams.....	58
Figure 67: Drill terminology	69
Figure 68: Schematic diagram and actual picture of the reference electrode.....	70
Figure 69: SEM picture for Titanium mesh (250X) for EDS analysis.....	71

List of Tables

Table 1: Probable anodic and cathodic reactions when steel embedded in concrete (C. M. Hansson, 1984; S. Ahmad, 2003)	10
Table 2: Features of the most widely used methods of corrosion monitoring in RC structures (P. Rodriguez, 1994)	12
Table 3: Corrosion rate (mpy) based on the linear polarization method (P. Venkatesan et al., 2006).....	16
Table 4: Nominal Compositions of steels (weight percent)	23
Table 5: Steel types with color code for the accelerated testing	28
Table 6: Steels used in the cracked ASTM A 955M specimen with the color code	34
Table 7 : Reference electrode potential with respect to SCE	70
Table 8 : EDS data after the analysis of the Titanium mesh	71
Table 9 : Concrete composition for beams and prisms	72
Table 10 : Actual composition of the rebar (weight percent) after analysis	73

1 Introduction

Corrosion of reinforcing materials is common problem in the North America due to de-icing salts. These de-icing salts have caused corrosion of the mild steel reinforcing bars (rebars) which then causes cracking and spalling of the concrete. In order to prevent premature deterioration of the structures, stainless steel rebars are being considered as alternatives to mild steel. A comparative evaluation has been made of these and the mild steel bars. The reinforcing steels under investigation are: regular and weldable mild steel (Grades 400 and 400W, respectively), and stainless steels: UNS 24100, 316LN, 2304 and LDX 2101.

The alternative grades of the steels were manufactured by varying of the percent contents of carbon, nitrogen, nickel, chromium, molybdenum, manganese, phosphorous, sulphur and silicon. Moreover, these alternative steels, of the compositions shown in Table 4, are designed to meet the strength requirements of structural rebar.

The costs of the reinforcing materials vary depending upon the compositions; regular and weldable mild steel being the cheapest, while the stainless steels are relatively expensive. Consequently, stainless steels are not commonly used in concrete structures or bridges because of the cost. The benefit of using stainless steel is that it gives higher corrosion resistance, and, thus, durability to the structures, for instance bridges and other structures. The bridge code in North Canada requires that the bridges should last for at least 75 years.

The main alloying constituent in stainless steel is chromium and at least 13% Cr (Monnartz P, 1911 quoted by Mary P Ryan et al., 2002) is required for the steel to be passivated by a layer of Cr_2O_3 . The other major alloying elements, nickel and molybdenum, are expensive. To reduce the cost of stainless steel, some of the nickel is replaced by manganese which is significantly cheaper.

Most of the highway structures in use are made of concrete; which is the most versatile material used around the world. Concrete is mainly made of aggregate, sand, cement and water. All the compositions have different effects on the concrete strength and durability. The strength of the concrete varies depending upon the water to cement ratio, and the admixtures used; the concrete gives the reinforcing materials the protective layer also. The water cement ratio plays an important role by controlling the porosity and, thereby, both the strength and the durability. The curing time for standard tests of concrete in laboratory is usually 28 days for the ordinary portland cement although shorter times are used in the field.

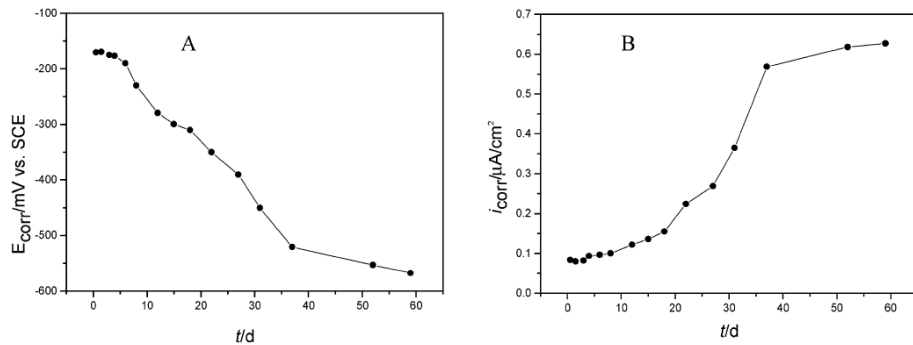


Figure 1: Variation of (A) the corrosion potential and (B) the corrosion current density of the reinforcing steel as a function of time for the specimen immersed in a 3.5 % NaCl solution (Rong-Gui Du et al., 2006)

The measurement of the corrosion potential and corrosion current density of the reinforcing steel was shown in the Figure 1; the corrosion potential of the reinforcing steel decreases; whereas, the corrosion current density of the reinforcing steel increases, both measurements were carried out with respect to the SCE (Rong-Gui Du et al., 2006).

Normally the corrosion potential, that is considered approximate threshold value for the initiation of corrosion, in the mild steel in concrete is -0.270 mV vs SCE. Under the experimental conditions of Rong-Gui Du et al., it is found the range for the corrosion initiation potential is greater than -0.22 passive; -0.22 to -0.27 active or passive; less

than -0.27 active (Rong-Gui Du et al., 2006). This is a narrower range than generally considered by ASTM C 876-09.

1.1 Reinforcing steels used for testing

Reinforcing steel like mild steel does not actively corrode in uncontaminated concrete which means concrete is the perfect environment for the steel. However, in Ontario more than 2 million tons of de-icing salts, containing ions of chlorides which penetrate into the concrete and cause active corrosion of the reinforcing steel, are placed on the roads and pavements each year during winter. Due to the corrosion, the corrosion products are formed on the reinforcing materials surface and, in some cases, the mild steel rebar is exposed from the concrete as the corrosion product forces the concrete to separate from the bar.

Because of the use of de-icing salts, there is premature deterioration of concrete structure such as bridges which contain mild steel. It is worth mentioning that the mild steels are produced from the scrap materials with the only specified components being limited to 0.5% P (Table 4) and called in the world of civil engineering as black steels (400) because of the black mill scale on the surface of the rebars.

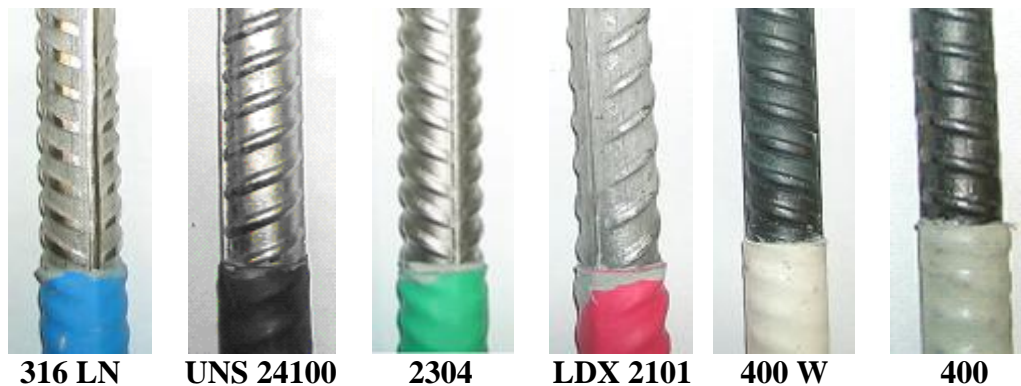


Figure 2: Different types of steels under investigation

To overcome the problem with mild steels in civil structures, the Ministry of Transportation of Ontario (MTO) would like to use stainless steel in areas of concrete

structures that are exposed to large amounts of chlorides. This is because stainless steel is more resistant to corrosion caused by de-icing salts than mild steels.

However, the traditional 316 LN stainless steel is very expensive because of the high cost of nickel and 316LN has high nickel content. Various manufacturers have developed alternative grades of stainless steels with low nickel content as described in the following section. So, the goal of this project is to evaluate the corrosion resistance of these alternative grades of stainless steels and black steels.

2 Literature review

2.1 Reinforced concrete:

Steel reinforced concrete used in structures gives strength and durability by having to bear both the tensile and compressive strength; whereas, the strength and durability vary depending upon the concrete and steel properties.



Figure 3: Failure surface in the case of pull-out failure of (a) a ribbed bar and (b) a smooth bar (K. Lundgren, 2007)

The bonding of the reinforcing steel with concrete is essential to allow transfer of load between these two components. The bond strength depends upon the types of rebar; ribbed or smooth due to the three different mechanisms: chemical adhesion, friction and mechanical interlocking. Among them, ribbed reinforcing has better bonding with the concrete surface due to increased friction and mechanical interlocking. As the corrosion products increase, the bonding capacity is increased for the smooth rebar until the cracking of concrete. The bonding of the ribbed rebar with the concrete can be increased to a certain extent, although bonding between the concrete and the reinforcing steel will be damaged in both cases (K. Lundgren, 2007).

Passive state is the state of the metal when the corrosion products form a protective film, limiting the rate of corrosion. The type of corrosion that mainly influences the surface of the steels in concrete is pitting corrosion, in which the passive film is destroyed locally and pits are formed on the surface of the steel. This reduces the strength along with the formation of reaction products in the form of rusts. Passivity can

be broken at critical chloride concentration depending upon the potentials of the steels (M. Moreno et al., 2004).

2.2 Properties of concrete

Concrete, which is a composite of cement, sand, aggregate and water; porous and brittle in nature, is the world's most widely used engineering material because of the availability and low cost. The strength of the concrete depends on the types of cements, sand, and aggregates, amount and types of admixtures and the water to cement ratio (P. K. Mehta, 1986).

To have different strength, sometimes portland cement is mixed in various proportions with several binders like silica fume, sulphate resistant, blast furnace slag (C. D. Lawrance, 1992), Moreover, various types of polymer fibers are added in the concrete to reduce the microcracking and, thus, have a better resistance to the corrosion process (P. Garcés et al., 2007).

During the mixing of the concrete; generally small, medium and large sizes of aggregates are used depending upon the requirement. In addition, it is found that calcium hydroxide which is a component of cement, is deposited around the aggregates, and can cause damage to the interfacial zone of the concrete also (D. Bonen, 1993).

Sands, which play a vital role in the strength of concrete, of various types such as natural river, coarse river, fine river, graded standard and standard sand, are determined depending upon the mass composition of gneiss, feldspar, limestone, quartz and others (Yan Fu et al., 1997).

Several types of admixtures, for instance accelerating, retarding, water reducing, plasticizers, air entraining, corrosion inhibitors, are used to produce concrete with different properties. The goal is to control the setting and hardened characteristics, surface tension of water, damage due to repeated freezing and thawing and, of course, rebar corrosion. However, the use of the admixtures increases the cost of the concrete

as they are very expensive. Moreover, concrete performance due to corrosion is also influenced by the type of admixtures used during the preparation of the concrete (A.A.A. Hassan et al., 2009).

The strength of concrete is directly controlled by the water to cement ratio: the lower the water to cement ratio, the higher the strength of the concrete and vice versa. The water to cement ratio also controls the porosity of the concrete (P. K. Mehta, 1986) along with the depth of the carbonated layers (H. Idrissi et al., 2003); in addition, the conductivity of concrete also varies depending upon the water-cement ratio, that is, the greater the water to cement ratio the more is the conductive path for ions to move inside the concrete.

2.3 Reinforcing steels

Reinforcing steel that is mostly used in construction industries is mild steel because of its low cost and ready availability, whereas, stainless steel is expensive because of its alloying constituents. The stainless steels consists of iron, carbon, nitrogen, chromium, nickel, molybdenum, manganese, phosphorus, sulphur, silicon with iron as the universal component of the steel as mentioned earlier. The other components are varied for the formation of the different grades of reinforcing steel. In addition, a common parameter for stainless steel is that it must have minimum 13% of chromium (Monnartz P, 1911 quoted by Mary P Ryan et al., 2002), which gives the resistance to corrosion; whereas regular black rebar, Grade 400, is specified only with a limit of 0.5% phosphorous and weldable black steel, Grade 400W, is required to have the following: 0.3% C, 1.6% Mn, 0.035% P, 0.045% S 0.5%Si, as indicated in Table 4.

During the manufacturing of steel, austenitic and ferritic regions are formed, which are visualized from the iron phase diagram; the austenitic regions are regulated in stainless steels by the use of the nickel (R. C. Newman, 2001). The protective layer on the stainless steel is created by chromium. However, to be effective, the chromium must be in solution but corrosion can occur by depleting of chromium at the grain boundary during high temperature exposure because of the formation of the chromium carbide,

Cr_{23}C_6 . To minimise this carbide formation, the carbon content of these steels is usually limited to 0.01 – 0.03%. Nitrogen is then added to provide alternative interstitial hardening. The resistance to pitting corrosion and passive film breakdown can be controlled by the use of Mo and Ni (M.F. Montemor et al, 1998).

2.3.i Benefits of using reinforcing steel

Reinforcing steels, from regular steel to stainless steels, give the strength and durability required for the concrete to withstand a tensile load at different levels, as concrete can only take compressive loads and is vulnerable to tensile loads. The cost of black reinforcing steel is cheaper than that of the stainless steel, but provides limited service life of structures exposed to chlorides. Stainless steels provide the extra corrosion resistance and can increase the service life of the concrete structures more than the expected service life obtained from the use of black steel (J. M. Frederiksen, 2009).

Corrosion is the most common degradation process in many parts of the world and can lead from simple aesthetic problems to catastrophic damage to the civil structures resulting in human casualty. The cost of the corrosion in concrete is twofold; direct cost, for instance, the direct annual cost of corrosion for the highway bridges in USA alone is \$ 6.43 to \$10.14 billion (M. Yunovich, 2001), and the indirect cost, which is even more than that of the direct cost. Among many other parameters for corrosion, reinforcing steels are the prime one and, by choosing the appropriate reinforcing steels, the cost of corrosion can be reduced.

2.4 Corrosion of reinforcing steel

Corrosion is the degradation of the metal or its alloys with the environment due to chemical attack, which consists of chemical or electrochemical reactions that depend on the transportation of electrons to and from the adjacent materials. Reinforcing steel in concrete is mainly black steel which can deteriorate predominantly because of corrosion.

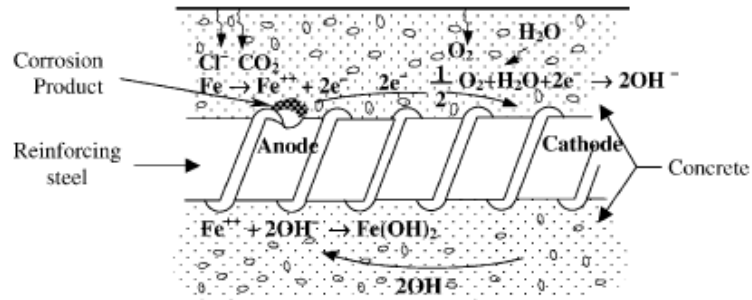


Figure 4: Schematic illustration of the corrosion of steel reinforcement in concrete – as an electrochemical process (Shamsad, 2003)

Corrosion of reinforcing steel is predominantly a result of the penetration of chloride into concrete (C. M. Hansson et al., 1985). Significant amounts of chloride come from de-icing salt used in the roads and bridges during winter. (A. A. Naqvia et al., 2006). Furthermore, the de-icing salt is primarily NaCl with impurities of unknown amounts such as MgSO₄, Na₂SO₄.

Reinforcing steel consists of iron as the universal component of the steel; corrosion of iron commences prominently by the anodic reaction and the related cathodic reaction which must occur simultaneously to have a complete reaction. When the reinforcing steel is embedded in concrete as shown by the schematic Figure 4 (S. Ahmad, 2003): both the anodic reaction where ferrous ion is formed and the cathodic reaction take place on the steel surface.

During these reactions, the electrons are transported through the rebar to the cathodic zone where they react with dissolved oxygen to produce (OH)⁻ which migrates through the concrete back to the anodic site to react with the ferrous ions and form the corrosion products or the oxides. In the absence of chlorides, the oxides are protective and steel is passivated. When chloride ions penetrate into the concrete, the corrosion products formed are not protective and active corrosion occurs.

As mentioned earlier, the corrosion of reinforcing steel in concrete is governed by iron and the corresponding anodic and cathodic reactions shown in the Figure 1, are not the

only reactions that form the oxides on the steel surface; the other anodic and cathodic reactions with the possible corrosion products when reinforcing steel embedded in the concrete are shown in Table 1; which depend on the pH of the concrete and the availability of the oxygen required to commence the reaction in the proximity (C. M. Hansson, 1984).

Anodic reactions	No	Cathodic reactions	No
$3\text{Fe} + 4\text{H}_2\text{O} \rightarrow \text{Fe}_3\text{O}_4 + 8\text{H}^+ + 8\text{e}^-$	(1)	$2\text{H}_2\text{O} + \text{O}_2 + 4\text{e}^- \rightarrow 4\text{OH}^-$	(5)
$2\text{Fe} + 3\text{H}_2\text{O} \rightarrow \text{Fe}_2\text{O}_3 + 6\text{H}^+ + 6\text{e}^-$	(2)	$2\text{H}^+ + 2\text{e}^- \rightarrow \text{H}_2$	(6)
$\text{Fe} + 2\text{H}_2\text{O} \rightarrow \text{HFeO}_2^- + 3\text{H}^+ + 2\text{e}^-$	(3)		
$\text{Fe} \rightarrow \text{Fe}^{++} + 2\text{e}^-$	(4)		

Table 1: Probable anodic and cathodic reactions when steel embedded in concrete (C. M. Hansson, 1984; S. Ahmad, 2003)

The suitable condition for iron in the passive state is shown by the equation (1) and (2), and when iron dissolves into ions are governed by the equation (3) & (4); while equation (5) is the cathodic reaction at high pH and equation (6) is the cathodic reaction at low pH (C. M. Hansson, 1984; S. Ahmad, 2003).

Even though common belief, corrosion process occurs due to the transfer of many electrons, formation of oxides, the oxides that are formed due to the anodic and cathodic reactions because of the exchange of the electrons, the corrosion process can occur even from a single transfer of the electron from the surface of the materials or surroundings (C. Alonso, 2001).

Stray currents can affect concrete not only depending on their composition but also the amount of available chloride content. Researchers have found the cause of the electrolytic corrosion more with the chloride in concrete as chloride is an aggravating agent for corrosion; whereas, passive reinforcement in concrete without carbonation and chloride usually offers resistant to stray current corrosion (L. Bertolini et al., 2007).

2.4.i Effect of chloride on reinforcing steel

Chloride, which is the main corrosive chemical for the reinforcing steels, comes from de-icing salts and the marine environment and destroys the passive film on the steel to cause the active corrosion by increasing the anodic reaction rate of the steel. The threshold of chloride may be defined as the minimum amount of chloride required to initiate active corrosion which is below the initial pitting corrosion potential.

In contrast, some researchers have found this definition of the chloride threshold is inconvenient with respect to the actual conditions, as the potential is measured at some specific points without consideration of area, postulating the requirement of considering the ratio between the active and passive areas of the corroding steels (C. Alonsoa et al., 2000). Moreover, comparison of the results of numerous methods of electrochemical tests for the threshold of chloride in concrete showed the variations in the data taken from different methods recommending to correlate the corrosion potential and chloride threshold value to find an optimum solution (L. Bertolini et al., 2008).

The threshold of chloride for rebar corrosion not only depends on the steel but also on many factors such as, concrete mix proportions, water cement ratio, steel surface condition, penetration time of the chloride. According to J. M. Frederickson (J. M. Frederickson, 2009), the threshold limit for chloride varies depending upon the limit of the distance or the thickness that the chloride has to travel; concluding that the penetration of chloride into the steels up to 30 mm may lead to 20 to 90 years of life; whereas, the nominal value for the penetration of chloride for the regular steel is 1 mm per year (B. Elsener, 2005).

The chloride threshold is also measured by the ratio Cl^-/OH^- , which is 0.6 for the black steel to initiate the corrosion (D. A. Hausmann, 1967 quoted by S. Wang et al., 2004); on the contrary, this ratio is negligible for the onset of corrosion in the stainless steel especially for 316LN which is ~ 11.6 or more (S. Wang et al., 2004).

2.4.ii Reinforcing steel electrochemistry

Many electrochemical measuring techniques for determining the behaviour of steel in concrete are noteworthy. Some of these are shown in Table 2 (P. Rodriguez, 1994) with the various characteristics, electrochemical methods are commonly used to measure the corrosion of the reinforcing steel: half-cell potential or potential mapping; electrochemical impedance spectroscopy (EIS), potentiostatic and potentiodynamic, electrical noise (EN)

Characteristic	Potential mapping	Concrete resistivity testing	Linear polarization method	Guard ring method	Coulometric method	Electrochemical noise method	EIS or A.C. Impedance method	Harmonics	Gravimetric test	Quantitative visual observation
Speed of individual measurements	A	A	A	A	A	B	B	B	C	C
Speed of response to change	A	A	A	A	A	A	A	A	C	C
Quantitative information	C	B	A	A	A	B	B	C	C	C
Non-destructive	A	A	A	A	A	A	A	A	C	C
Non-perturbing	A	C	C	C	B	A	B	C	C	C
Measurement parameter	Probability of corrosion	Probability of corrosion	I _{corr}	I _{corr}	I _{corr}	I _{corr}	I _{corr}	I _{corr}	Average I _{corr}	Geometrical feature of attack

“A” instantaneous (optimum), “B” fairly slow (satisfactory), “C” very slow (un-satisfactory).

Table 2: Features of the most widely used methods of corrosion monitoring in RC structures (P. Rodriguez, 1994)

Half-cell potential or corrosion potential is the quantitative measurement of the potential difference between reinforcing steels and a standard reference electrode. It is a qualitative indication of whether the steel is corroding or not and, when measured over a given area under investigation, potential maps can be obtained. Potential mapping (ASTM C 876) is the portrait of the anodic and cathodic portions and only provides information on the probability of whether the steel reinforcement is in passive state or is actively corroding.

During the process of half-cell potential measurement of the materials, the surface of concrete has to be sufficiently wet so that there is a low resistance path between the rebar and the reference electrode in the concrete surface. Although half-cell measurement is the most popular technique used for the measurement of the corrosion of reinforcing steel in practice, it does not give enough information about corrosion in progress (S. Ahmad, 2003). Therefore, care should be taken during the half cell measurement to take into account other factors, the surrounding environment of the reinforced concrete; preferably the test is carried out repeatedly round the year (A. Poursaee et al., 2009).

Polarisation, which can be static or dynamic depending upon the nature of the application of the potential or current, is the term given to the situation when the voltage or current is changed from the equilibrium potential or current. If the potential or current applied during polarization is kept fixed to a certain value, the polarization is called potentiostatic polarization; whereas, the potential or the current is increased continuously either positive or negative mode, the polarization is called potentiodynamic polarization.

The cyclic polarization technique was introduced in the 1960's and modified during 1970's (D. C. Silverman, 1998) to a fairly simple technique. In this method, the potential is applied between the working electrode, the metal to be tested, and the reference electrode at a continuous rate; the respective current between the working electrode and counter electrode is measured. While measuring the cyclic polarization, the potential is generally increased in the anodic direction from the corrosion potential to a potential several hundred millivolts more positive than the corrosion potential and the scan is reversed back, once the desired potential is reached.

The cyclic polarization is more aggressive than other scans available because of the greater range of polarization and interpretation of the polarization result is difficult. It is generally assumed that the application of the polarization causes no change in corrosion mechanism through a significant potential range (D. C. Silverman, 1998), nevertheless,

some researchers postulate that cyclic polarisation is the most informative electrochemical test (A. Poursaee et al., 2009).

2.5 Effect of corrosion products on the reinforcing steel

Corrosion products are the oxides or hydroxides formed on reinforcing steels due to anodic dissolution of steels. They affect the reinforcing steels as well as concrete structures by reducing its cross section and, therefore, its strength and durability. In addition, with the increase of the corrosion products, the corrosion rate is reduced because of the hindrance caused by the corrosion products to have more oxygen available for the further progress of corrosion reactions (T. El Maaddawy et al., 2007).

Moreover, the corrosion products are formed over local areas leaving pits in the rebar. This can also happen for stainless steel in concrete, reducing the metal thickness. The pits may be shallow or deep depending upon the corrosion and the placement of metals in the environment. In reinforced concrete in practice, they are usually relatively shallow and can be extensive along the bar. When the pits are deep, it is really hard to separate the stainless steel corrosion current density and corrosion products with computer topography (M. Beck et al, 2009).

When corrosion products are formed on the reinforcing steel inside the concrete, the hydroxyl ions are also consumed faster by the corrosion products to fulfill the competition with the chloride ions (S. Wang et al., 2004).

2.5.i Reduction in strength

The effects of reinforcement corrosion on the strength of the reinforced structures can be evaluated by three factors: the losses in the effective cross-sectional area of the concrete due to the cracking of the concrete cover (Araki et al. 2007); the losses in the mechanical performance of reinforcement due to its reduced cross-sectional areas (P. Rodriguez, 1996); and the losses in the bond strength and rigidity between corroded

reinforcements and concrete (C. Fanga, 2006; K.Y. Kim et al., 1998; Lee et al. 2002; Han-Seung Lee et al., 2009).

The cross sectional area or the thickness of the reinforcing steel decreases (P. K. Mehta, 1993) due to the formation of oxides during the corrosion process, that is, the loss of the metal from the surface or inside the steels and reduction in the mechanical strength (O. Poupard et al., 2006; Han-Seung Lee et al., 2009); which are more prevalent in the black steel than in stainless steel. As the corrosion rate is very slow in stainless steel, it actually retains the strength to hold the structure despite the formation of the corrosion products even after long time of exposure in harmful environments (J. Cairns et al., 2007).

2.5.ii Prevention of the corrosion

Corrosion of reinforcing steel can be prevented by using concrete having three properties: a highly alkaline pore solution inside the concrete which will help to maintain the passive film of the reinforcing steel; low porosity and low permeability that will reduce the penetration of the harmful chemicals for instance, chloride; and high electrical resistivity that will reduce the flow of ions into the concrete electrons from anode to cathode (D. Chen et al., 2008).

Patch repairing for a concrete structure is shown schematically in Figure 5: the reinforcing steel was treated after removing the corrosion products and patching material is placed around the reinforcing steel as cover. Patch repairing is a common process which leads to the formation of the ring anode effect that is, the corrosion between the substrate and the patched repaired concrete or in the interface of the concrete and reinforcing steel (J. Zhang et al., 2006).

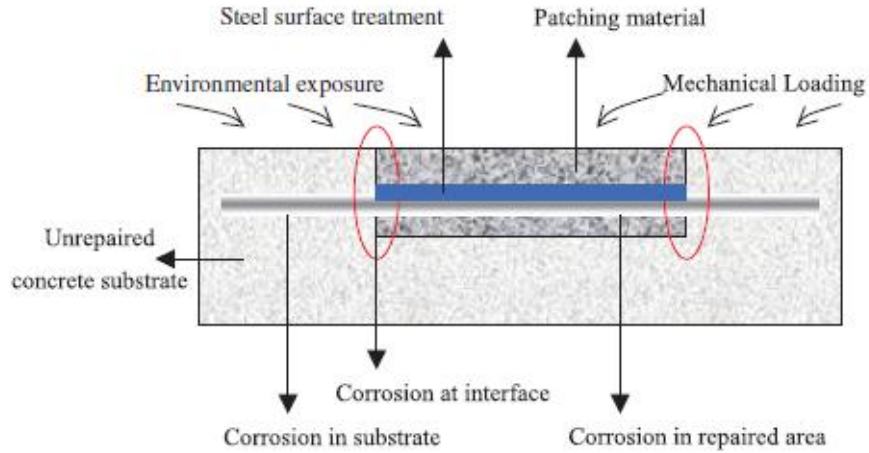


Figure 5: Steel corrosion process and current flow in concrete (J. Zhang et al., 2006)

To prevent further corrosion in the reinforcing steel, one or all of the following things must be done: to block or retard the anodic process; to block or reduce the cathodic process and to reduce the transportation of ions the electrolyte in the concrete; which is also true for the patch repairing of the concrete (RILEM, 1994).

Level	Mild steel plain(control) bar	CPCC coated bar	IP net coated bar	Epoxy coated bar
Atmospheric	0.0001	0.000	0.0008	0.0013
High tide	0.0281	0.0066	0.0088	0.0101
Seafloor	0.0201	0.0011	0.0021	0.0033

Table 3: Corrosion rate (mpy) based on the liner polarization method (P. Venkatesan et al., 2006)

Coating reinforcing steels with paint or epoxy is another way to reduce the corrosion of the reinforcing steels inside; which may lead to increased corrosion of the steels by absorbing the moisture from the surrounding environment more, if the moisture gets inside the concrete. P. Venkatesan et al. found when mild steel inside the concrete is placed without coating and with coating using three different epoxies on the reinforcing steels in concrete namely, cement polymer epoxy coating(CPCC), interpreting polymer network coating (IPN) and epoxy coating (EC) gives better resistance to corrosion in

atmospheric, high tide and sea floor environment, as can be seen from the linear polarization data shown below in Table 3 (P. Venkatesan et al., 2006)

Sometimes $\text{Ca}(\text{NO}_2)_2$ is added to the concrete as a corrosion inhibitor and is found to reduce the corrosion of the reinforcing steel significantly both in not cracked and cracked concrete cover, when concrete is prepared according to the ACI standard 318 (N.S. Berke et al., 1993).

2.6 Concrete degradation and its effects

Corrosion of concrete is primarily governed by concrete carbonation and chloride penetration (O. Poupard et al., 2006,), both of them commence due to the variation of the concrete compositions, chemicals and surrounding environments (O. Poupard et al., 2006). Concrete carbonation is the process when carbon di-oxide from air gets into the concrete and reacts with the $\text{Ca}(\text{OH})_2$ to form calcium carbonate; the rate of carbonation depends on the water cement ratio, cement content, curing period, porosity and strength. The pH of the concrete is reduced not only by the carbonation process but also by other acidic gases coming from the adjacent environments, like SO_2 and NO_2 ; this reduction of the pH is harmful for the embedded reinforcing steels in concrete (S. Ahmad, 2003).

Chloride, which is always a dangerous ingredient for the concrete structures described in detail in the following section, damages any concrete structure by reducing the strength and durability of the materials. It can even cause severe damage in compressive strengths of the concrete also (W. Morris et al., 2004), depending on the cation, for instance Na, Ca or Mg (A. Poursaee et al., 2009).

2.6.i Effect of chloride on concrete

Chloride is the deadly ingredient that causes the deterioration for the concrete structures due to the formation of the corrosion products on the reinforcing steel. Concrete normally has the pH of 12.5 to 13.5, which is equivalent to that of the pore solution, and chloride ion can replace the hydroxyl ion in the concrete by reducing the pH of the concrete.

Further, when the chloride ions gets into the concrete and destroys the passive film of the reinforcement, the pH of the concrete is lowered inside the concrete; which induce corrosion of the reinforcing steels (L. L. Mammoliti, 1996). Chloride not only reduces the hydroxyl ions but also increases the moisture content of the concrete, which increases the corrosion rate making more oxygen available for the anodic reaction. After certain time the corrosion rate decreases with the increase of the corrosion products as those starts acting as a barrier for further chemical reactions to commence.

Moreover, chloride increases the electrical conductivity of the concrete, which increases the transportation of the electrons to carry out the anodic and cathodic reactions needed for the corrosion of the reinforcing steel.

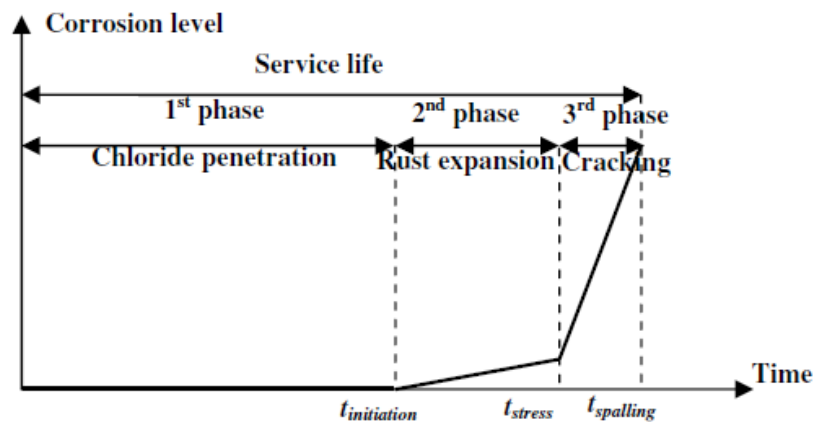


Figure 6: Chloride induced reinforcement corrosion process (D. Chen et al., 2008)

Chloride penetration in the concrete can be described by three phases as shown in Figure 6: in the first phase, it penetrates inside the concrete from the surrounding environment and corrosion of reinforcement starts as soon as the critical threshold value

of chloride is reached; in the second phase, the products on the reinforcing steel increases in volume that is, expansion of the products; finally, the rust causes the cracking of the concrete structures (D. Chen et al., 2008).

2.6.ii Cracking of the concrete

Cracking of concrete occurs mainly due to formation of the corrosion products of the reinforcing materials by electrochemical reactions and various loading conditions surrounding the structure, whereas, cracks in the concrete can be enlarged by the expansive pressure of the corrosion products; in other words, cracking occurs as corrosion products pressurize the interface of the rust band and corrosion product, which occupies more volume than the original reinforcing bar (D. Chen et al., 2008).

There may be three cases for cylinders to cause the crack because of the corrosion products – not cracked, partially cracked and cracked: in the not cracked concrete, there is less chance to have ions or harmful chemicals to get into the surface of the reinforcing materials; whereas, for the partially cracked concrete, there is a chance for the harmful chemicals to get inside the concrete faster, there is a limitation of the critical mechanical opening (30 μ m) which prevents diffusion of any ions regardless of the age of the concrete (M. Ismail, 2008), and finally for cracked concrete, it is easier for any impurities to diffuse and cause corrosion of the reinforcing materials.

As mentioned previously, the pH plays a vital role for the corrosion of the concrete and the reinforcing steel; when the pH is lowered, the passive film loses its protective capacity. Along with that high porosity and permeability can reduce the strength and can cause cracking and spalling of the concrete (P. K. Mehta, 1986).

2.7 Microcell and Macrocell corrosion:

Microcell corrosion, a ubiquitous state for all the reinforcing steel in concrete or with adjacent environment, causes corrosion; when anodic reaction takes place in the metals due to the exchange of the electrons and the cathodic reaction taking place on the adjoining part of the same metal surface (P. Rodríguez, 1999; C.M. Hansson et al., 2006).

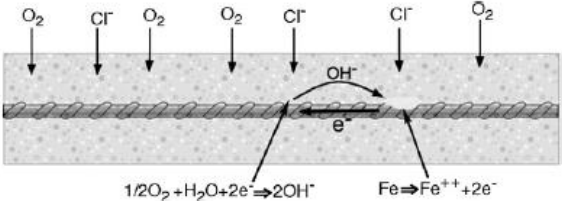


Figure 7: Schematic illustration of microcell corrosion (C. M. Hansson et al., 2006)

The microcell corrosion was illustrated schematically in Figure 7; the anodic reaction causing the electrons to transfer on the same metal surface to the cathodic zone and causing the reduction of the dissolved oxygen to form hydroxyl ion, while oxygen and chloride ions are getting inside the concrete from the outside environment. In addition, microcell corrosion deteriorates the reinforcing steel due to the formation of the corrosion product, which can cause concrete cracking depending upon the amount of the corrosion product as well as spalling of the concrete.

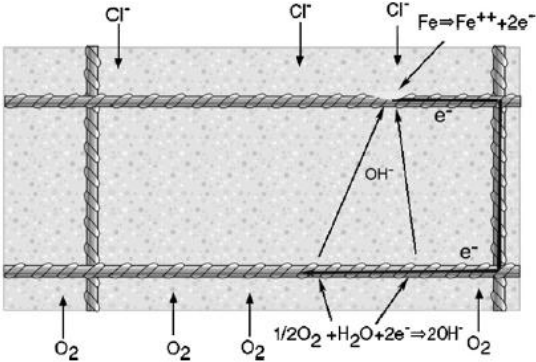


Figure 8: Schematic illustration of macrocell corrosion (C. M. Hansson et al., 2006)

Macrocell corrosion, in other words, galvanic corrosion, is the anodic reaction commencing between two reinforcing steels placed apart; one acting as active, that is

anode, and the other one as passive, that is cathode (L. Bertolini, 2009), because of the diverse environment or the compositions of the reinforcing steels (P. Rodríguez, 1999; C.M. Hansson et al., 2006). On the basis of most postulations, generally macrocell corrosion is considered to occur between two reinforcing steels inside the concrete, which can be seen from the schematic illustration in Figure 8; whereas, researchers have found that it can even occur between single reinforcing steel and the surrounding environment (C. M. Hansson et al., 2006).

In macrocell corrosion, not only the anodic and cathodic reactions occur separately on two reinforcing steels but also can occur simultaneously on both the reinforcing steels; whereas, one of the reinforcing steel is more active, that is, acts as an anode to have the macrocell couple (C.M. Hansson et al., 2006). Moreover, C. Andrade et al. found that the presence of macrocell couple in the reinforcing steels does not necessarily eliminate the microcell corrosion process; which occurs on the surface of the reinforcing metal as mentioned previously (C. Andrade, 1992).

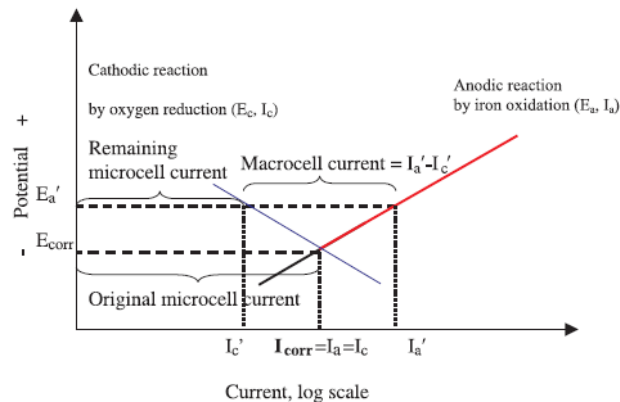


Figure 9: Schematic microcell and macrocell corrosion of the active steel (J. Zhang et al., 2006)

Figure 9 illustrates the microcell and macrocell corrosion of the active steel by Evans diagram, showing the corrosion potential, E_{corr} and the corrosion current, I_{corr} ; when the anodic and cathodic reactions were in equilibrium and the microcell current that was measured by different methods as shown in the Table 2.

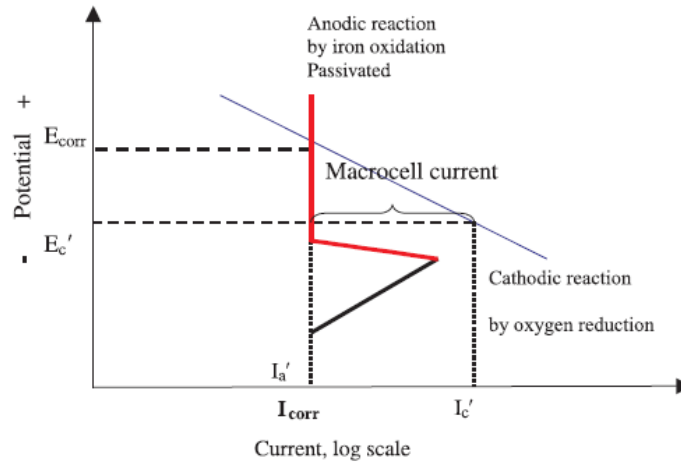


Figure 10: Schematic microcell and macrocell corrosion of the passive steel (J. Zhang et al., 2006)

In addition, macrocell current, ($I_{\text{macro}} = I_{a'} - I_{c'}$) that was generated when the potential of the active steel was increased to $E_{a'}$ between the two reinforcing steels as the active steel was generating more current to be supplied to the passive steel, which cannot consume more electrons are shown in the Figure 10. In the case of the passive steel, the macrocell couple consumes more electron than the amount of electrons can be supplied from the active steel.

2.8 Concluding remarks

The corrosion of the reinforcing steel in concrete varies depending upon the concrete and steels in use. The variation depends on many factors including concrete mixture, aggregate size, steels, and environments. Many researchers have found many criteria of measuring and preventing corrosion in practical and research field. Some of them sometimes give ambiguous results showing that further research has to be carried out for better understanding of the corrosion of steels in concrete.

3 Experimental procedure

3.1 Types of reinforcing steels:

Six different reinforcing materials were investigated: two austenitic stainless steels: UNS 24100 (Enduramet 32) and 316LN, two duplex stainless steels; 2304 and LDX 2101 and two black steels; 400 W and 400. UNS 24100 & 316LN stainless steels were supplied by Valbruna Canada Limited; 2304 & LDX 2101 by Outokumpu, UK; 400 W from Gerdau Ameristeel, Canada and 400 by Mittal, Canada.

The nominal compositions of the six different types of steel are shown in Table 4 with the percentages of the different constituting materials in the steels. The most expensive components of these steels are Cr, Ni and Mo, whereas manganese is relatively inexpensive.

Steel Types	C	N	Cr	Ni	Mo	Mn	P	S	Si
316LN	0.02	0.14	17.2	10.3	2.1				
UNS 24100	0.06	0.2-0.45	16.5-19	0.5-2.5		11-14	0.06	0.03	1.0
2304	0.02	0.17	22	5.7	3.1				
LDX 2101	0.03	0.22	21.5	1.5	0.3	5.0			
400 W	0.3					1.6	0.035	0.045	0.5
400							0.5		

Table 4: Nominal Compositions of steels (weight percent)

Even though very expensive, the percent compositions in Table 4 show that 316 LN contains Mo along with greater percentages of Ni and Cr, which makes it more resistant to corrosion and one of the most widely used stainless steel alloys in the field. The LN stands for low carbon and high nitrogen; adding nitrogen gives the strength to compensate the loss of the strength incurred due to reducing the carbon in the steel as well as the resistance to corrosion.

The austenitic steel UNS 24100 also known as Enduramet 32® Carpenter. It has low nickel content, no molybdenum and the large amount of manganese making it cheaper than the other stainless steels while retaining the austenitic structure. The Chromium content gives the resistance to corrosion to the materials by creating a protective film. However, if Cr is depleted on the grain boundary of the steels, the chance of corrosion increases and the process is called sensitization due to the precipitation of chromium carbide in the grain boundary during the exposure to high temperature.

The duplex steel, 2304 and LDX 2101 have both austenitic and ferritic phases; they both have high chromium, providing resistance to the corrosion like other stainless steels. LDX 2101 has less amount of Ni, Cr and Mo, which makes it less expensive than 2304.

400 is the normal black rebar that is mostly used in concrete structure; 400 is the minimum yield strength in MPa. Mostly the corrosion data present in the research field are for this steel which is used with confidence and the testing of the black steels in this project was performed to compare the change in corrosion behaviour with respect to the current available data of mild steels. Along with that the testing of the 400 W. W conforms that the material can be used in special circumstances where weldability and ductility are required, which has more stringent composition specifications for comparing the performance of 400 W to that of 400 steels.

3.2 Accelerated testing of the reinforcing steel

As mentioned previously, corrosion is a slow degradation process for reinforcing materials in corrosive environment where and it takes normally many years for the reinforcing materials to corrode completely. Since four of the steels that were being tested were steels that could tolerate large amounts of chlorides, it was necessary to design a system for enhancing the rate of chloride penetration into concrete without unduly influencing the behavior of the steels. Various types of accelerated corrosion tests have been used to simulate the situation in the laboratory within short period; accelerated corrosion testing of rebar is done preferably in mortars or concrete with the

presence of corroding environments or chemicals like CaCl_2 , NaCl , MgCl_2 mixed with the concrete or mortar. A common procedure is to apply an anodic current to the embedded rebar (or polarize it to a fixed potential) while exposing it to a chloride solution in which is placed the cathode. The chlorides are, thus, accelerated under the electric field into the concrete to the rebar. There are many disadvantages to this procedure because it changes the environment around the rebar (A. Poursaee and C. M. Hansson, 2009). Consequently, an alternative technique was devised in which there are two external electrodes, a cathode placed in a chloride solution in a ponding well on top of the specimen and an anode in a bath into which the specimen is placed.

Subsequent to the construction of the specimens, described below, the same method has been described by M. C. Alonso et al. There are two types of accelerated corrosion test, potentiostatic and migration method. In the potentiostatic method, the reinforcing materials are polarised to a fixed potential; whereas, in the migration method, the potentials are applied between two external electrodes placed in two different electrolytes. The survey of literature shows that there are two noticeable variations in the migration methods of accelerated corrosion testing: Migration I method is that where the rebar is embedded inside the concrete and the two external electrodes are placed outside; whereas, in migration II is the embedment of the anode in the cementitious materials or concrete that is one electrode inside the concrete (M. C. Alonso, 2009).

The accelerated test in this project corresponded to the migration method I where the applied potentials was 500 mV which was in between +500 mV to -500 mV selected according to the Pourbaix diagram of iron (M. Pourbaix, 1974). Pourbaix diagram for iron showed that the oxides of iron were stable in between the selected potentials indicating a lower possibility for active corrosion. The tests performed on the beams were; open circuit potentials and linear polarization resistance, on a cycle basis. The cycle for the tests consisted of seven days, six days of which potential was applied on the beams and one day without the application of the potentials to depolarize all the rebar embedded in the concrete.

3.2.i Design of the test beams

The designs available for the accelerated corrosion testing in the literature show that the placement of the rebar in different positions discussed, as follows, affects the corrosion data. The first design in consideration was; the six rebar was placed in the vertical position in one side having ponding well right beside the rebar with the reference electrode embedded in the middle of the beam. Along with that, the electrodes for applying the potential were thought to be placed in the ponding well and underneath the test beams.

However, the problem associated with this design was the placement of the ponding well right beside the rebars which could hinder the migration of the chloride ions, the NaCl solution to represent the de-icing salts, on the side surfaces of the rebar inside the concrete directly. Moreover, the placement of the ponding well right beside the rebar was increasing the volume of the beams under consideration leading to a more bulky specimen to be tested in the lab.

While considering the second design, the rebar was placed one underneath another and the reference electrode was placed in the center in between the two layers of the rebar. Like the first design under consideration, the ponding well was thought to be placed on the top of the beam with the electrodes for applying the potentials.

Although the placement of the rebar could lead to a longer period of the diffusion of the chloride ions to the underneath rebar as chloride will migrate to the top rebar first. Along with this limitation, there will be generation of macrocell corrosion as the design was supposed to be for the accelerated microcell corrosion.

The final design selected by the author after discussions with the research group with the help of the group members used for the accelerated corrosion testing is shown in Figure 11. In this design, six sections of rebar of the same types of steels along with the reference electrode were placed side by side equidistantly, one and half inch, having reference electrode in the center. The dimension of the beam selected was 457.2 mm ×

228.6 mm × 247.7 mm and that of the ponding well was 381 mm × 152.4 mm × 63.5 mm placed in the center of the beam.

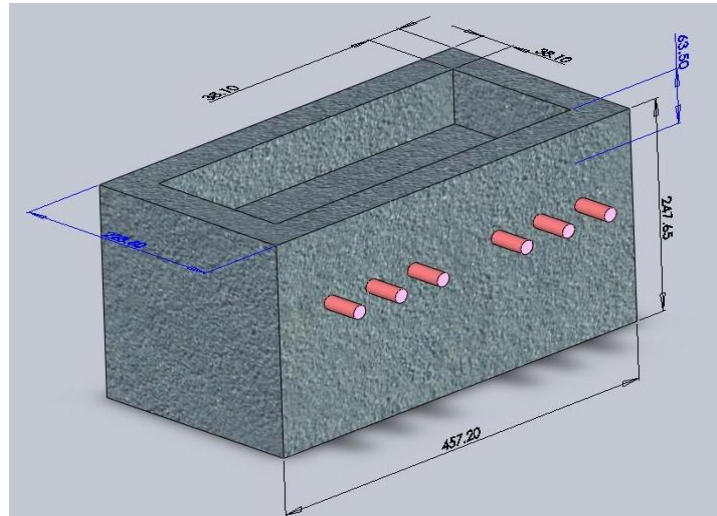


Figure 11: Final accelerated corrosion measurement design for the beams

The placement of the rebar and reference electrodes were underneath the ponding well which was 25.4 mm below from the bottom of the ponding well. The reference electrode which used was Mn/MnO₂ (ERE 20), supplied by the Force Technology and described in detail in Appendix B from page 70, could be embedded in the concrete in wet and dry condition both in chloride and chloride free concrete. Moreover, the potentials measured by this reference electrode do not vary with the chemical properties of the concrete, which is why, corrosion potentials are not affected by the potentials of the reference electrode.

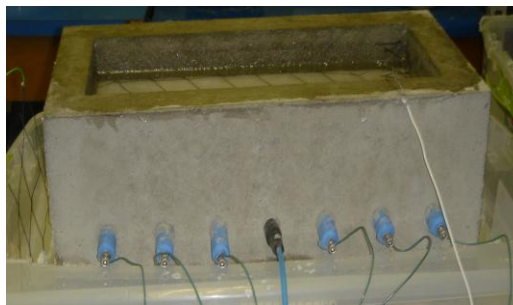


Figure 12: One of the six beams under investigation

A photograph Figure 12, of one of the beams shows all the rebar coloured in blue, the black reference electrode and the titanium mesh electrodes for applying potential – one on the top in the ponding well and one below the beam in the trough. To simulate the practical conditions that a concrete structure faces, the ponding well was filled with saturated NaCl and the trough was filled to a depth of 1000 mm with the saturated Ca(OH)₂ solution to prevent leaching of the hydroxyl ions from the concrete beams.

The concrete cover over the reinforcing materials was 25.4 mm in thickness conforming to the ASTM Standard C 876-09. According to the standard, while designing the concrete cover has to be not more than 76.2 mm so that the measurement of the open circuit potential is convenient enough to compare the data with the other available data for the same materials.

3.2.ii Preparation of the test specimens

The ribbed rebar grades were colour coded as shown in Table 5. The both ends of the bars were faced by using a lathe machine to have uniform surface; the rebars were then drilled and tapped, 19.05 mm.

Steel Type	Color code	Bar Size (metric/nominal diameter in mm)	Quantity of each rebar
UNS 24100	Black	15M/16	06
316LN	Blue		
2304	Green		
LDX 2101	Red		
400 W	White		
400	Transparent		

Table 5: Steel types with color code for the accelerated testing

The stainless steel screws, Holo-Krome Socket head cap screw 10-32 UNRF of 25.4 mm in length inserted to provide connection to an electrical lead, while the other end of the rebar was sealed to have no connection with the surrounding environment. To have an uninterrupted connection between the rebar with the parstat, equipment used for

corrosion measurement in this case for open circuit potential and linear polarization resistance, all the screws were connected to external wires and/or alligator clips.

After cleaning the rebar surfaces with alcohol both ends of the rebar was coated with two layers of Sikafloor® 261^A epoxy for a length of 76.2 mm. The shrink fit tubing was applied to the bars to give additional protection. For the final preparation, all the rebar was hot glued at both ends of the bars leaving 152.4 mm of bare surface and 76.2 mm of coating at each end.

3.2.iii Casting of the concrete

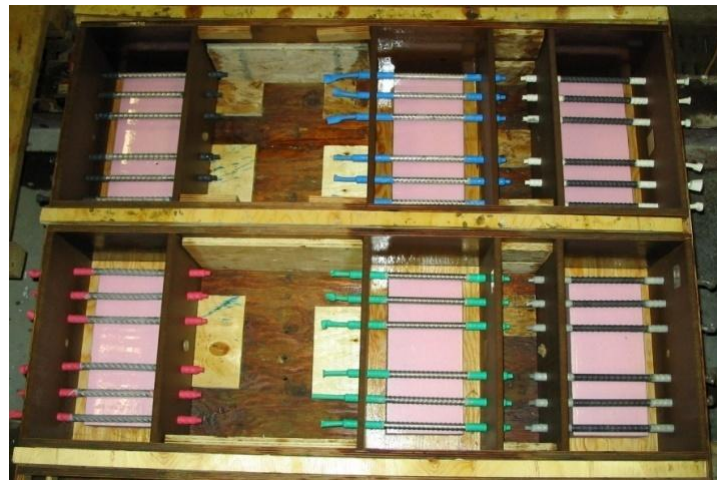


Figure 13: Formwork made for the beams

In Figure 13, the final formwork is shown with all the bars and reference electrode in place. The casting was done using the concrete mix according to the CSA Class F-1 standard (Appendix D) supplied by Dufferin Concrete. The slump for the concrete was 6.8 mm, which gives the flowability of the concrete and the air content was 6.6% giving the amount of void spaces available for the concrete after casting for expansion. The water cement ratio for the concrete used was 0.45.

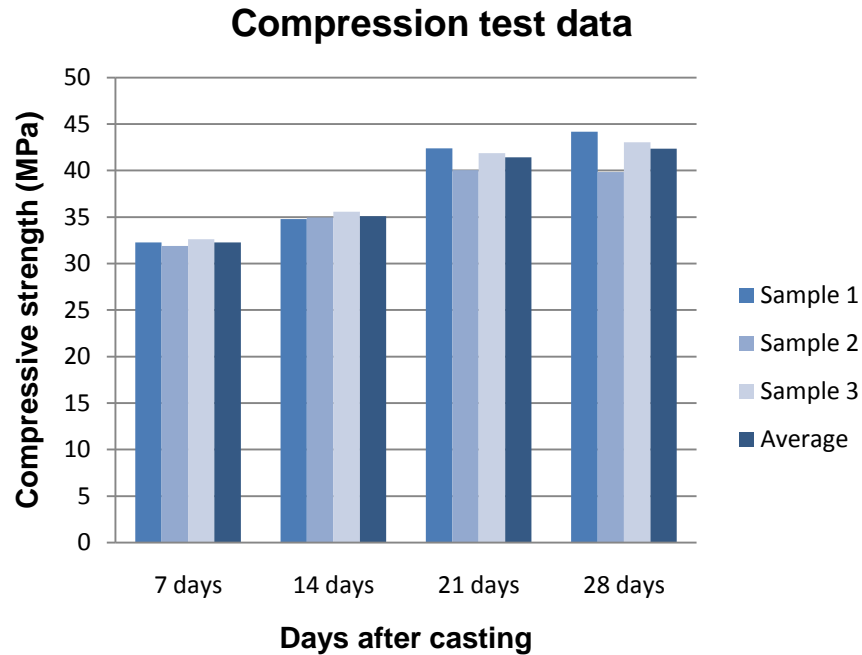


Figure 14: Compressive strength of the cylinders for the beams

The compressive strength data of the cylinders made from the concrete used for the beams are shown in the Figure 19: the comparison of the compressive strength data after each week showed the compressive strength of the cylinders increasing with time after the casting until 28days and became constant.

3.2.iv Accelerated corrosion test setup and corrosion measurement of the reinforcing steel

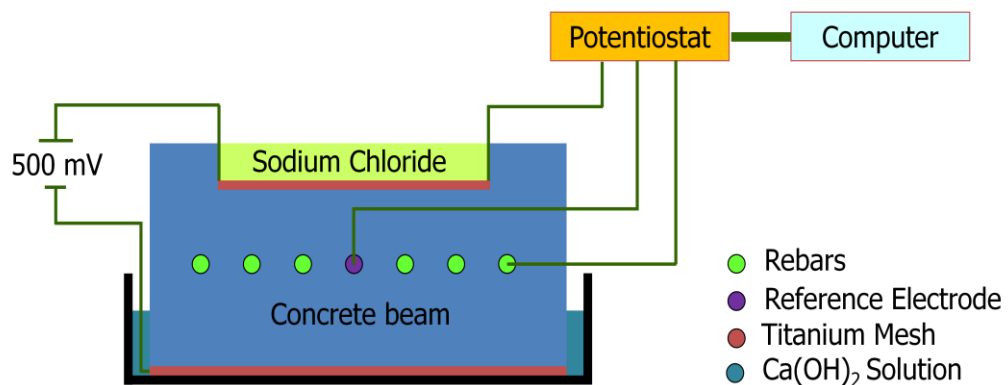


Figure 15: Schematic accelerated corrosion test setup and wiring diagram

The Figure 15 shows the schematic experimental set-up for the accelerated corrosion test for one beam of the six beams in total. As mentioned previously, six beams of similar dimension and setup were made with six reinforcing steels of the same type in each of the beam. The bars are shown as green circles and the red circle shows reference electrode that was embedded in the concrete. The beams were placed in a plastic container shown by the black lines with saturated Ca(OH)_2 solution to prevent leaching of hydroxyl ions from the concrete. The titanium meshes, which acted as electrodes for the power supply were placed in the ponding well and in the bottom of the container. The titanium mesh in the ponding well was also used as the counter electrode during the corrosion measurement.

Diffusion of the chloride ions into the concrete requires long time due to the porosity and permeability of the concrete and in the case of stainless steels, a large amount of chlorides in the concrete is required to induce corrosion. Therefore, to increase the chloride penetration rate into the concrete, a 500 mV potential was applied between the two titanium meshes to cause the chloride to migrate from cathode in the ponding well to anode below the beam.

During the corrosion measurement, which was in this case linear polarization resistance described below, the rebar acted as the working electrode, the titanium mesh in the ponding well as the counter electrode and Mn/MnO₂ as a reference electrode embedded in the beam. The power supply was disconnected 24 hours before performing the corrosion measuring test during which, the corrosion measuring unit potentiostat (EG & G from Princeton Applied Research) was connected to a computer as shown in Figure 15. The potentiostat measures the potential and the current using the software (Power Suite®) which was able to perform potentiostatic, potentiodynamic, cyclic polarisation according to the requirement.

3.2.v Electrochemical techniques used for the testing of steel

The corrosion measurement that was performed for the accelerated corrosion testing is called linear polarization resistance (LPR). In this measurement: the corrosion potentials (E_{Corr}) of the bars were measured between the rebar and reference electrode, then a 20 mV potential more positive than the corrosion potential was applied between the rebar and counter electrode (the titanium mesh in the ponding well); thereafter, a 20 mV potential more negative than the corrosion potential was applied, as shown in the Figure 16, the polarization periods were 150 seconds, providing time for the resulting current for both the application to reach the steady state.

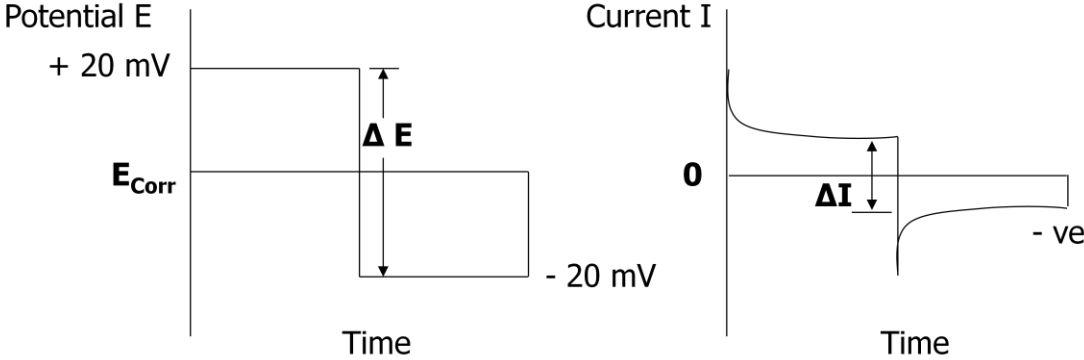


Figure 16: Linear polarization resistance principle

All the above information was used in the following two equations by M. Stern and A.L. Geary (1957), J. Electrochemical Society 104 (1).

$$R_p = \Delta E / \Delta I \dots\dots\dots (3.i)$$

$$i_{Corr} = B / (R_p * A) \dots\dots\dots (3.ii)$$

To calculate the polarization resistance (R_p), the total applied potential (40mV), is divided by the difference in the steady state current (3.i). Then the corrosion current density, i_{Corr} , was calculated by using the obtained R_p value in the equation 3.ii, where A is the total exposed corroding area of the rebar in consideration and B is the Tafel constant.

3.3 Macrocell monitoring of the reinforcing steel in cracked concrete

3.3.i Design used for testing

The ASTM G 109 prism is designed to simulate bridge decks having multiple rebar mats, and has one bar in the top and two bars in the bottom. To simulate cracks that might generate in the bridge decks or concrete structure ASTM A 955/A 955M-07a (A3- cracked beam test) was used; the design has been slightly modified in lateral dimensions to meet the casting situation in the laboratory, prepared with crack to be parallel and above the top rebar for faster migration of the chloride, whereas, this design was specifically for the highly corrosive resistant rebar to accelerate the ingress of the chloride.

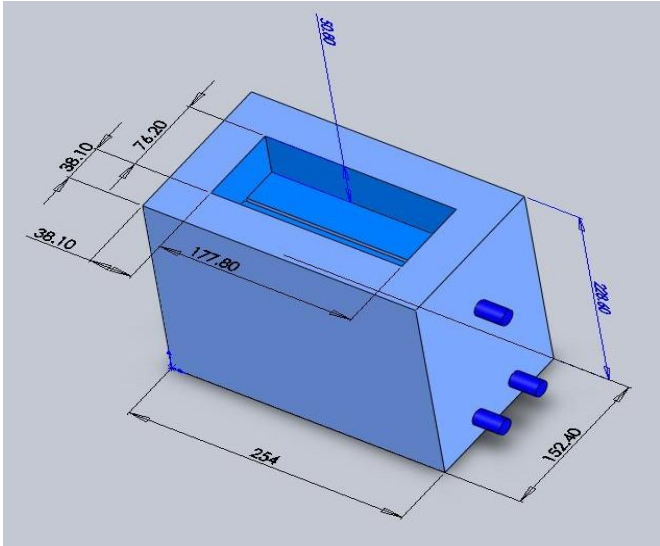


Figure 17: Schematic illustration of the specimen design (ASTM A 955M)

The design specified for the cracked beams as per ASTM standard specification for deformed and plain stainless steel bars for concrete reinforcement (ASTM A955M) is shown in the Figure 17. The prism had a ponding well on the top with the crack of 0.30 mm, in the center directly on the top of the rebar touching the center of the rebar while the top rebar was placed 25.4 mm below from the bottom of the ponding well. The bottom two bars in the prism were placed 152.4 mm below the top rebar two inch equidistantly apart from the corners of the prism; the length of the top and bottom rebar

was 304.8 mm, while the dimension of the prism and ponding well were 254 mm × 152.4 mm × 228.6 mm and 177.8 mm × 76.2 mm × 50.8 mm respectively.

3.3.ii Preparation of the test materials

The rebar for the macrocell tests were prepared according to the procedure mentioned in the section 3.2 ii. The top and bottom rebar for the ASTM A955/A 955M-07a cracked beam test along with bar types, bar size, color code and are shown in the Table 6. All of the bottom rebar consists of black steel (400) in total sixty in numbers having color code in black and yellow.

Top Bar Steel Type	Color Code	Bottom Bar Steel Type	Color Code	Bar Size (metric/nominal diameter in mm)	Quantity of beams per steel grade
UNS 24100	Black	400	Black/ Yellow	15 / 16	5
316LN	Blue				
2304	Green				
LDX 2101	Red				
400 W	White				
400	Transparent				

Table 6: Steels used in the cracked ASTM A 955M specimen with the color code

During the preparation of the ASTM A 955M cracked prisms; shims of thickness of 0.30 mm of 152.4 mm width were used to produce the “crack”. The shims were cut to the size of 114.3 mm length bending the shim to 12.7 mm as shown in the Figure 18; the bending of the shim was done to provide additional support to generate the crack in the center.



Figure 18: Picture of the shim used for casting of the prisms

Before the testing of the corrosion rate, the two bottom rebar was connected with 18 gauge wires and 10 ohm resistors were soldered with the alligator clip to be connected to the slot of the Keithley for the automatic measurement.

3.3.iii Casting of the materials

Stainless steel shims of width 152.4 mm and 0.3 mm were cut to a length of 114.3 mm and 19.05 mm of 114.3 mm were bent to 90°. The 90° bending of the shim gave additional strength for the bottom wood and foam to hold concrete pressure, and was placed in between the styrofoam and bottom wood. The same styrofoam that was used to make ponds for the beams with a dimension of 76.2 mm × 50.8 mm × 63.5 mm were used for casting of the prisms having two pieces of the styrofoam glued and screwed in the center of the bottom wood with the stainless shim in the wood to have firm joint.



Figure 19: Form work for the casting of the ASTM A 955M prisms

During the final assembly, the formwork was oiled along with the shim to make sure that concrete does not stick with the side planks, bottom woods and shims, after that the rebar was placed in the holes of the planks making sure that the top rebar touch the shim in the center of the bare six inch length as shown in Figure 19.

The concrete used for casting prisms was supplied by Dufferin concrete (Appendix D) according to the following standard specifications as per ASTM A 955M for one cubic yard; 355 kg of type I portland cement, 160 kg of water, aggregate with 32.5% of the

total concrete volume, air content $6\pm 1\%$. The specimens were cast upside down in two layers and each layer of concrete was vibrated for 30 seconds; finishing the surfaces of the bottom side of the prisms with wooden float. The prisms were removed from the formwork after one day, while the shim was removed by the hydraulic press, and cured with distilled water in plastic bags for three days. The prisms were dried in the air for 25 days and the vertical surfaces of the prisms were then sanded with emery paper and cleaned thoroughly for the epoxy coating.

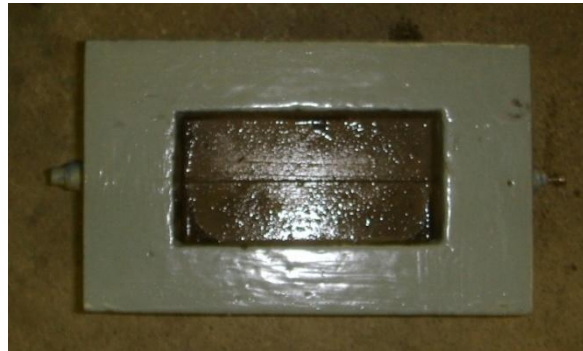


Figure 20: Top surface of the actual prism after the coating

The prisms were coated with the primer BASF Nitoprime®30 and left for 4 hours to dry; then two layers of epoxy coat of BASF Swerguard® HBS 100 was given as shown in Figure 20.

3.3.iv Macrocell corrosion setup and measurement

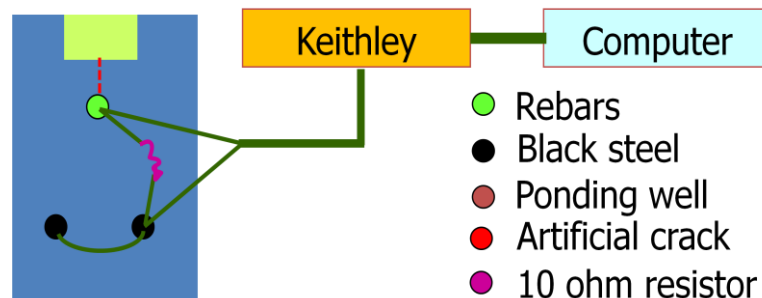


Figure 21: Schematic setup of the ASTM A 955M prism

The schematic diagram is shown in the Figure 21 of the cracked prism test along with the entire component used for the measurement. The crack in the prism was artificially created to penetrate the chloride solution to the rebar center surface directly from the ponding well on the top of the prism. The green circle shows the top rebar whose corrosion rate was being measured; both the bottom rebar made with black steels were connected together with 18 gauge electrical wires to have equal potential. To measure the corrosion rate, 10 ohm resistors were connected between the top and bottom bars for automatic measurements of the potential drop between the top and bottom rebar by using data acquisition apparatus which measures sequentially the potential drop between the bars of individual prisms connected to its specific slots as shown in the Figure 22.



Figure 22: Actual picture of the cracked prism with the setup

Because of the artificial crack, the chlorides can directly go to the steel surface. To simulate the practical environmental conditions, the bars were passed through cycles of wetting and drying. A cycle consists of seven days of sequential wetting and drying of which three days are dry and four days are ponding with salt solution; the salt solution used was 15% NaCl by mass. On the first day of a cycle, the ponding is done by the NaCl solution for four days at room temperature; and after four days of the ponding the potential drop was measured through the 10 ohm resistors and the corrosion rate was calculated according to the equation (3.iii). The solutions were then vacuumed after 4 days and the prisms were dried for three days under heat tent. The cycle was repeated for 12 weeks followed by 12 weeks of continuous ponding to complete 60 weeks of testing. The ASTM A 955M (Cracked beam test) specifies maintaining a temperature $38^{\circ}\text{C} \pm 2^{\circ}\text{C}$; whereas, the temperature was maintained in the lab was room temperature

27 °C. The open circuit potentials of the top rebar was taken after two hours of drying and after two days during the drying period according to the standard ASTM C 876-09.

3.3.v Electrochemical techniques used for the measurement

The electrochemical techniques used for macrocell measurement were the potential mapping, the corrosion rate by voltage drop as described below and linear polarization resistance. The potential mapping was done according to the ASTM C876-09.

The corrosion rate for the embedded steel was measured using the following formula

$$\text{Rate} = 11.6 * i_c = \frac{11600 V}{A.R} \quad (\mu\text{m}/\text{yr}) \dots\dots\dots (3.iii)$$

Where:

i_c = corrosion current density ($\mu\text{A}/\text{cm}^2$)

V = voltage drop across resistor (mV)

R = resistance of the resistor (ohms)

A = area of exposed metal at the anode bar (cm^2)

The resistor used is 10ohm with ½ kilowatt power capacity. For the linear polarisation measurement of the macrocell prisms, the corrosion rate was calculated in mA/m^2 or $\mu\text{A}/\text{cm}^2$ using the equations 3.i and 3.ii sequentially as described in 3.2 iv.

4 Experimental results and discussion

4.1 Corrosion of the reinforcing steel under accelerated test

4.1.i Microcell corrosion

The corrosion current density for the 316 LN shows that, after 400 days of exposure in the accelerated environment, the corrosion current density remains in the range of the 0.01 to 0.10 mA/m². This can be converted to average reduction in cross section of the steel using Faraday's Law. In this case, the corresponding rates are 0.0116 to 0.116 μm/year. The corrosion current densities for the UNS 24100, 2304 and LDX 2101 remained between the range of 0.05 to 0.20 mA/m² (0.0058 to 0.232 μm/year) which is slightly higher than that of 316LN. The corrosion current densities are shown in the Figures 23 to Figure 26.

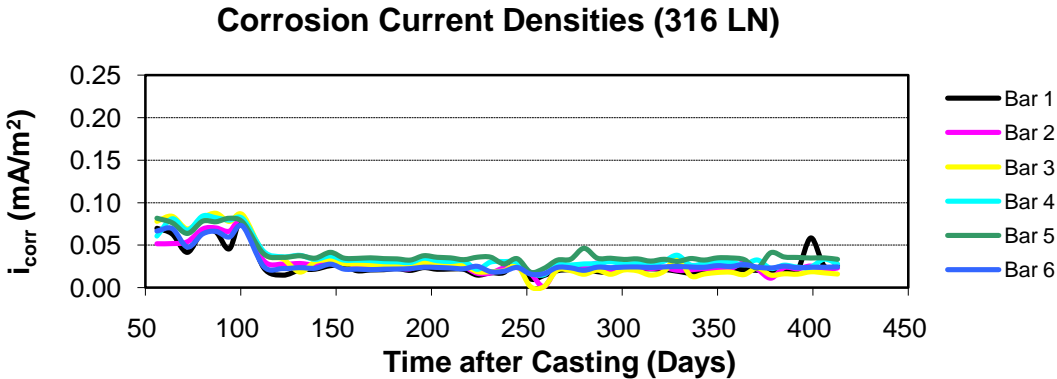


Figure 23: Microcell corrosion current density for 316 LN rebar in beams

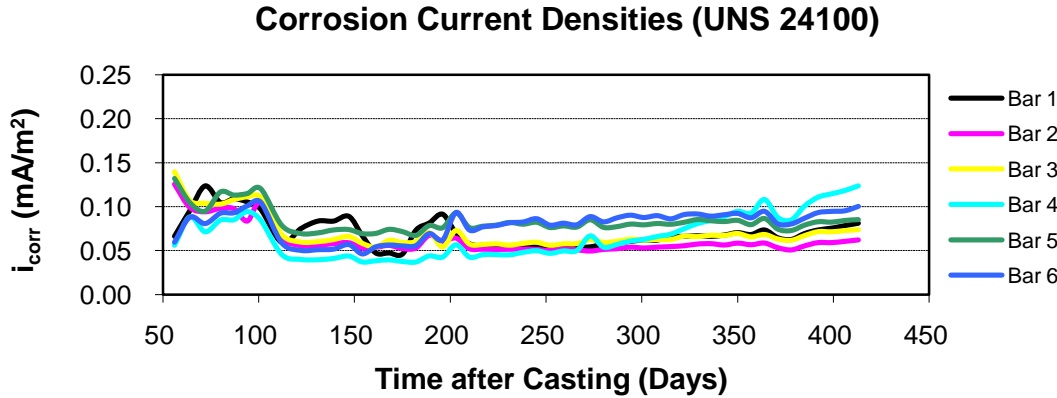


Figure 24: Microcell corrosion current density for UNS 24100 rebar in beams

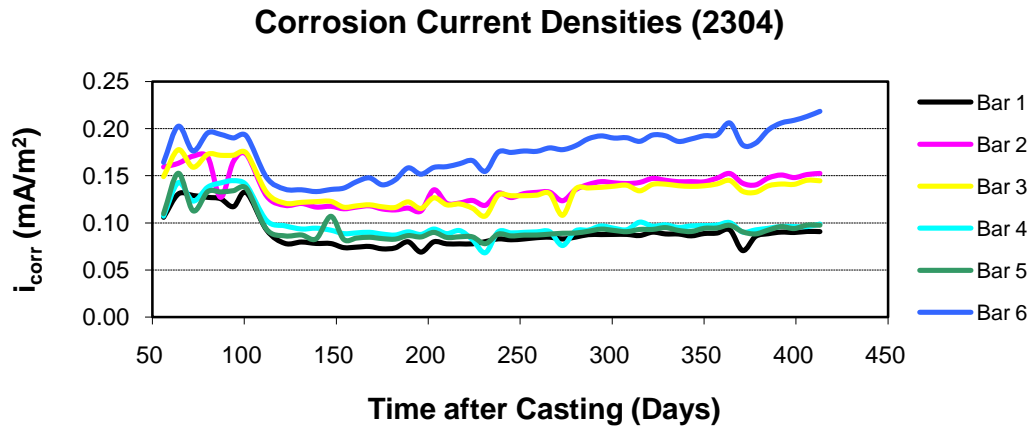


Figure 25: Microcell corrosion current density for 2304 rebar in beams

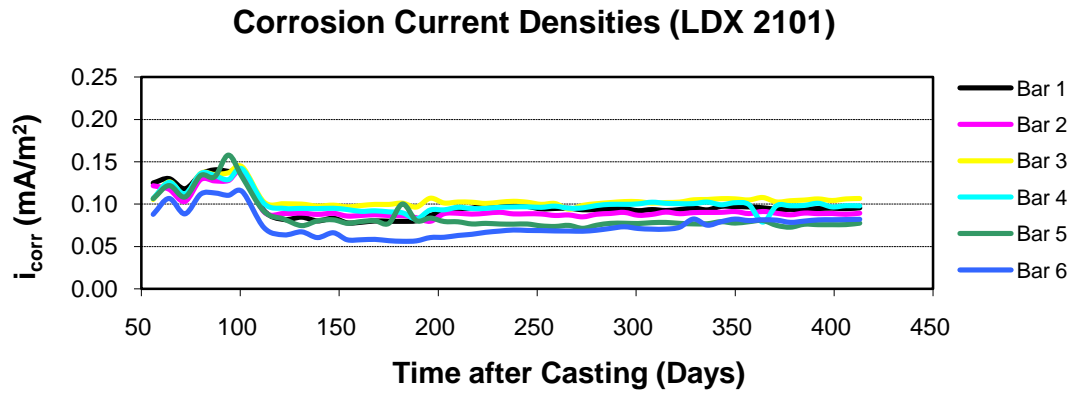


Figure 26: Microcell corrosion current density for LDX 2101 rebar in beams

The minor drop in corrosion rate of the stainless steels at 120 days after casting is due to removal of a layer of solid NaCl which had precipitated at the bottom of the ponding wells, effectively adding an electrical resistance to the circuit.

Initiation of corrosion in five bars the Grade 400 ranged over a long period. This is attributed to the inhomogeneous nature of concrete and the uneven penetration of chlorides. The corrosion current densities for 400 and 400 W increase over time to a level of 2 to 7 mA/m² (2.32- 8.12 μm/year) as shown in the Figures 27 and 28.

Corrosion Current Densities (400 W)

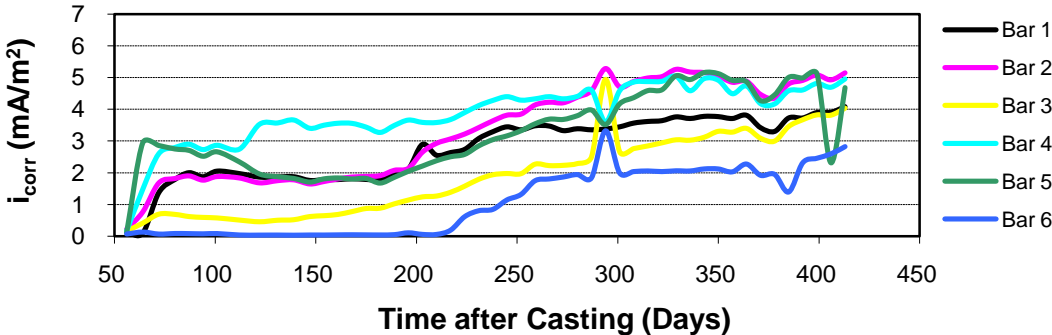


Figure 27: Microcell corrosion current density for 400 W rebar in beams

Corrosion Current Densities (400)

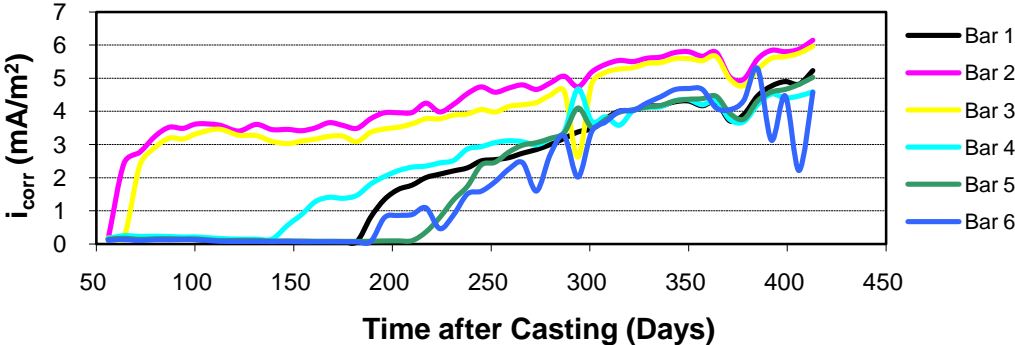


Figure 28: Microcell corrosion current density for 400 rebar in beams

4.1.ii Corrosion potential

The corrosion potentials of all the stainless steels was ~ -200 mV SCE which corresponds approximately to the equilibrium potential between solid Cr_2O_3 and dissolved CrO_4^{2-} ions at a pH of ~ 13.5 (M. Pourbaix, 1974). Figure 29, for the 316 LN, shows that the corrosion potential dropped in the first few weeks then remains between -100 to -300 mV SCE after 430 days of exposure in accelerated corrosion environment. This indicates that the potentials of these steels are very different from those of mild steel; a potential of -300 SCE would represent a probability the some of the steel had begun to corrode but the autopsied 316LN bars showed no sign of corrosion. On the other hand, the corrosion potential for the UNS 24100 remained between -50 to -150 mV SCE, which would be indicative of a low probability of corrosion in mild steel and, indeed, there was no corrosion on the autopsied UNS 24100 bars.

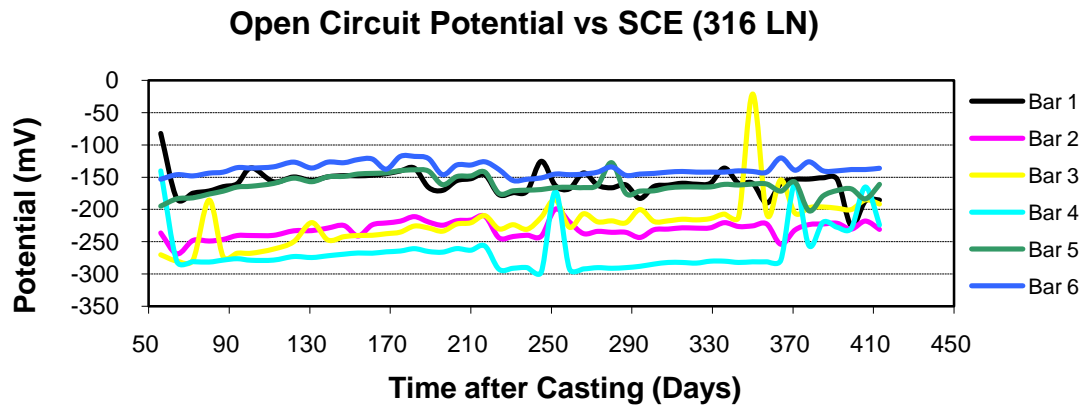


Figure 29: Corrosion potential for 316 LN bars in beams

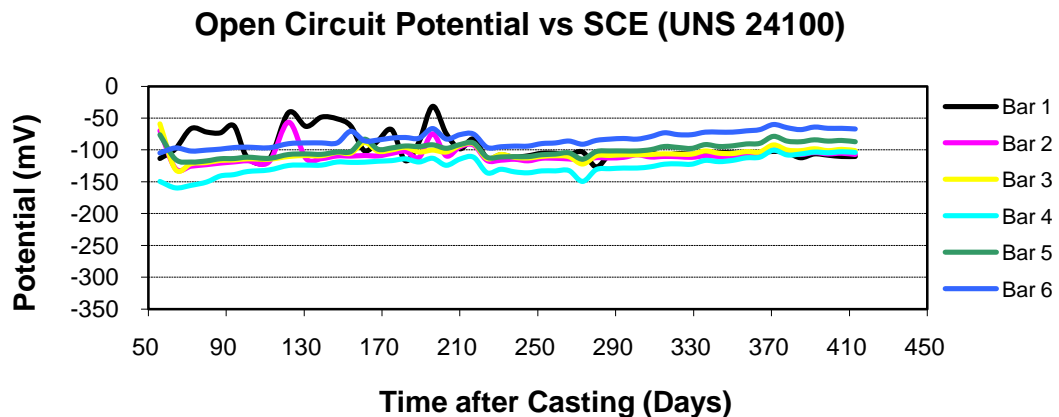


Figure 30: Corrosion potential for UNS 24100 bars in beams

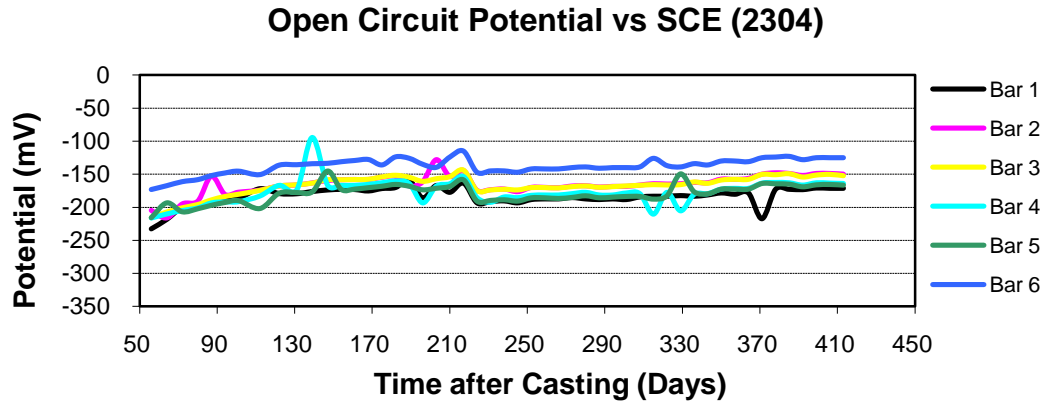


Figure 31: Corrosion potential for 2304 bars in beams

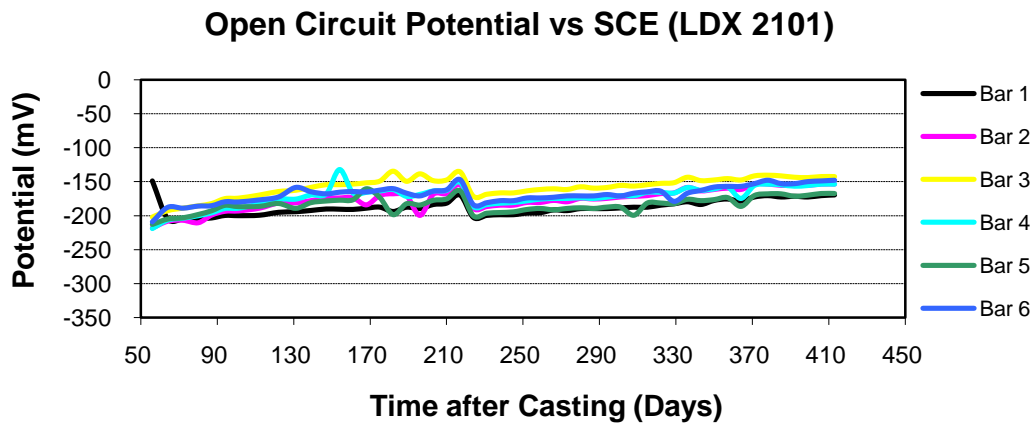


Figure 32: Corrosion potential for LDX 2101 bars in beams

The corrosion potential for the 2304 steel bars lie between -100 and -200 mV, and that of LDX 2101 in between -150 and -200 mV. These alloys, too, have less nickel and more manganese than the 316LN. Both of these are duplex steels with both the ferritic and austenitic phases

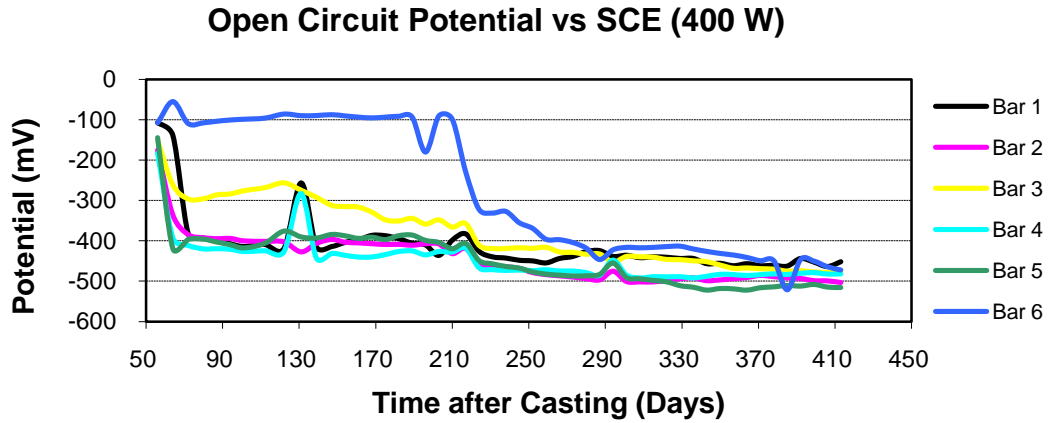


Figure 33: Corrosion potential for 400 W bars in beams

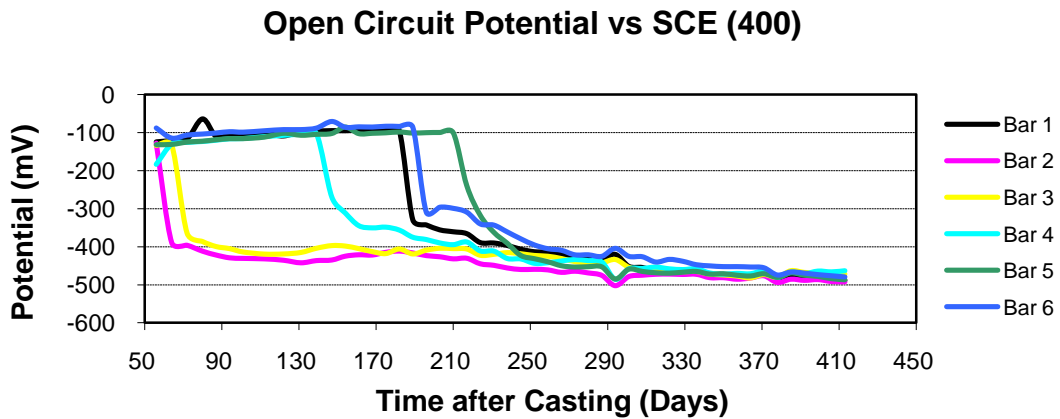


Figure 34: Corrosion potential for 400 bars in beams

For black steel, it is considered that potentials more negative than -350 mV CSE) (-230 mV SCE) are indicative of active corrosion. Figure 33 shows that five of the six 400 W steel bars started actively corroding within two weeks of exposure to the accelerated environment and the potential dropped from -100 to -500 mV sharply. The corrosion potentials for the 400 indicate that, initially the corrosion started for two bars after 64 days and rest started corroding around 180 days as shown in Figure 34, in agreement with the corrosion current densities given in Figures 27 and 28.

4.1.iii Visual inspection of the reinforcement for the beams

Three bars are removed from each beam for visual inspection and micrographs are shown in the figures below







Bar No.	Top View	Underside View
1		
2		
3		

Figure 35: Surface of 316 LN bars after breaking open three bars from the beams







Bar No.	Top View	Underside View
1		
2		
3		

Figure 36: Surface of UNS 24100 bars after breaking open three bars from the beams

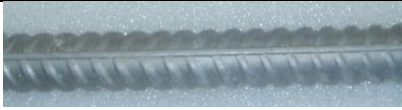
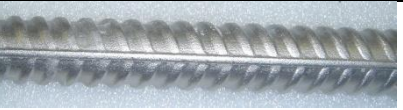

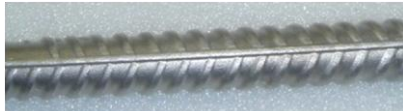


Bar No.	Top View	Underside View
1		
2		
3		

Figure 37: Surface of 2304 bars after breaking open three bars from the beams







Bar No.	Top View	Underside View
1		
2		
3		

Figure 38: Surface of LDX 2101 bars after breaking open three bars from the beams

The surface image of the UNS 24100, 316LN, 2304 and LDX 2101 are shown in the Figure 35 to Figure 38; they did not show any visible sign of corrosion on the surface of the rebar.







Bar No.	Front View	Rear View
1		
2		
3		

Figure 39: Surface of 400 W bars after breaking open three bars from the beams







Bar No.	Front View	Rear View
1		
2		
3		

Figure 40: Surface of 400 bars after breaking open three bars from the beams

Severe amount of rust was found on the surfaces of the 400 and 400 W bars especially on the top of the bar, that is, closest to the ponding surface, whereas, the underside surface of the bars remained relatively free from corrosion as shown in Figures 39 and 40.

4.2 Macrocell corrosion of the reinforcing steel under accelerated test

4.2.i Macrocell corrosion

The macrocell corrosion current density for the 316 LN shows that after 200 days of exposure in 15% chloride solution with wet and dry cycle as per ASTM A 955M, the corrosion current densities remain in the range of the 0.01 to 0.3 $\mu\text{m}/\text{yr}$ which can be shown in the Figure 41.

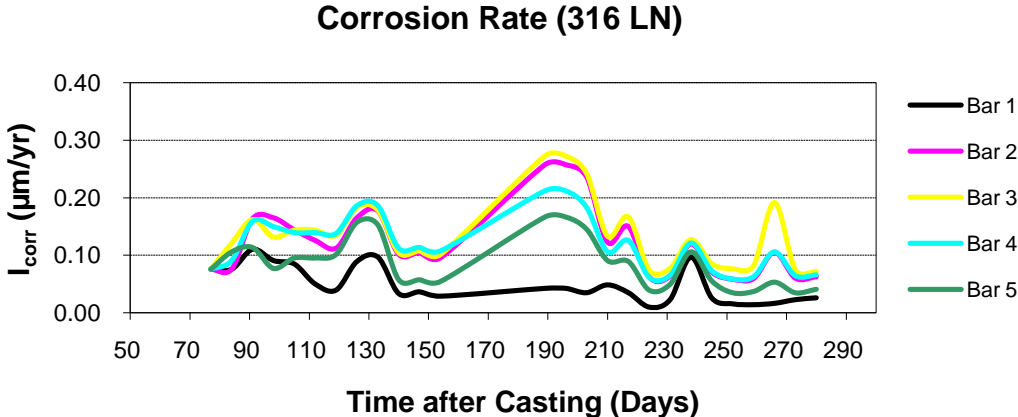


Figure 41: Macrocell corrosion current density for 316 LN rebar in prisms

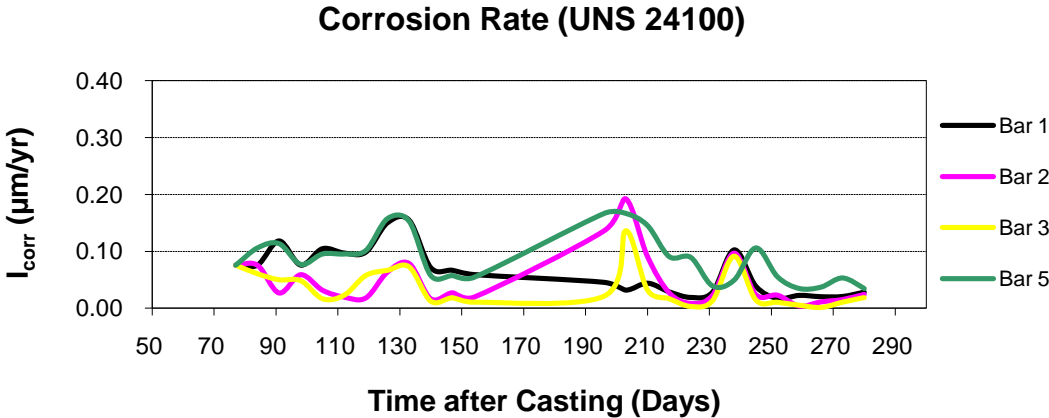


Figure 42: Macrocell corrosion current density for UNS 24100 rebar in prisms

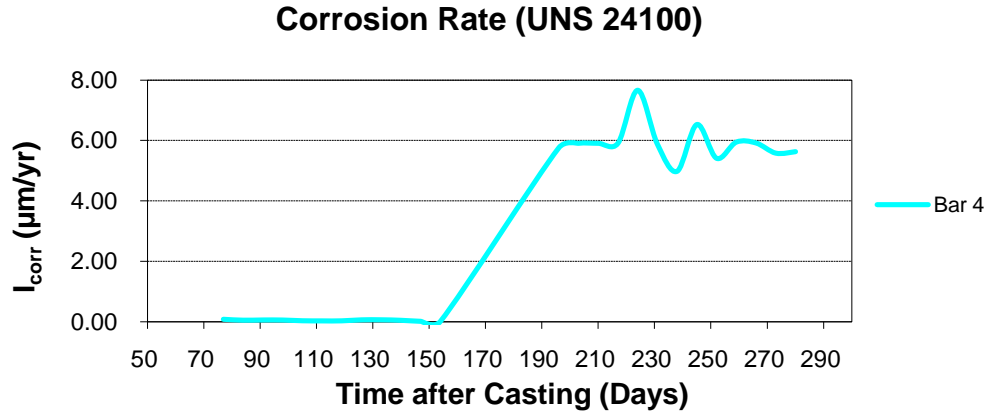


Figure 43: Macrocell corrosion current density for UNS 24100 rebar 4 in prisms

The macrocell corrosion current density for UNS 24100 is in the range from 0.01 to 1 $\mu\text{m}/\text{yr}$ as shown in Figure 42, except for bar 4 for which corrosion rate increased from the base corrosion rate to 6 $\mu\text{m}/\text{yr}$ and remained steady as in Figure 43 which is attributed to a large void in the casting. As shown in Figure 44 and 45, the corrosion rate for 2304 and LDX 2101 were found to be up to a maximum of 0.3 $\mu\text{m}/\text{yr}$.

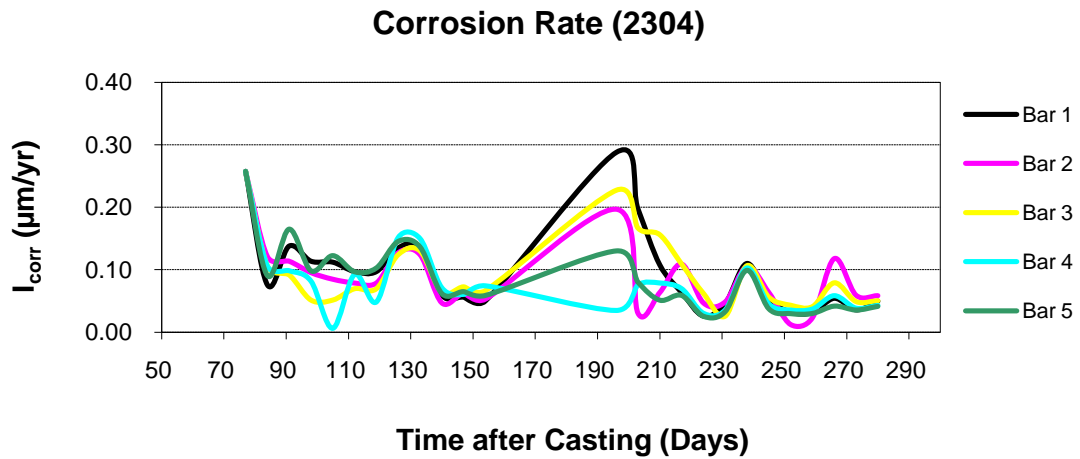


Figure 44: Macrocell corrosion current density for 2304 rebar in prisms

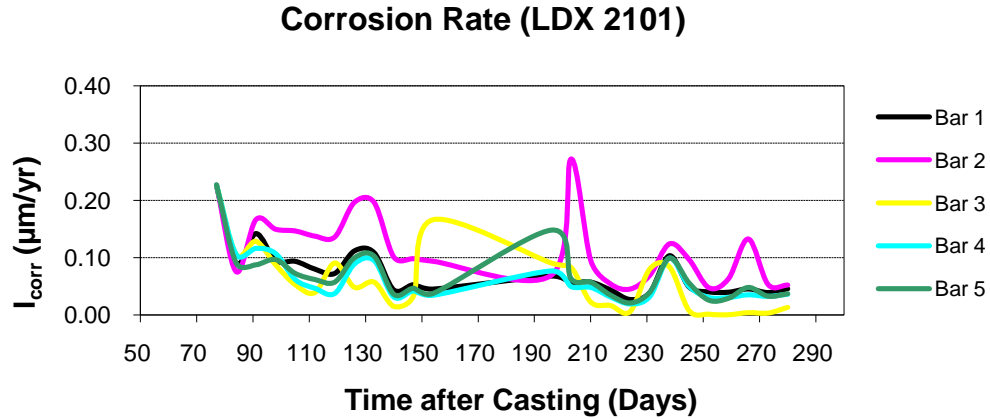


Figure 45: Macrocell corrosion current density for LDX 2101 rebar in prisms

The macrocell corrosion current density for the 400 and 400W show that the corrosion rate increased rapidly initially then decrease over the next 200 days of exposure in 15% chloride solution. The decrease is probably due to a reduction in the oxygen content of the concrete as a result of the cathodic half cell reaction., The maximum corrosion rate was $\sim 30 \mu\text{m}/\text{yr}$ as shown in the Figures 46 and Figure 47.

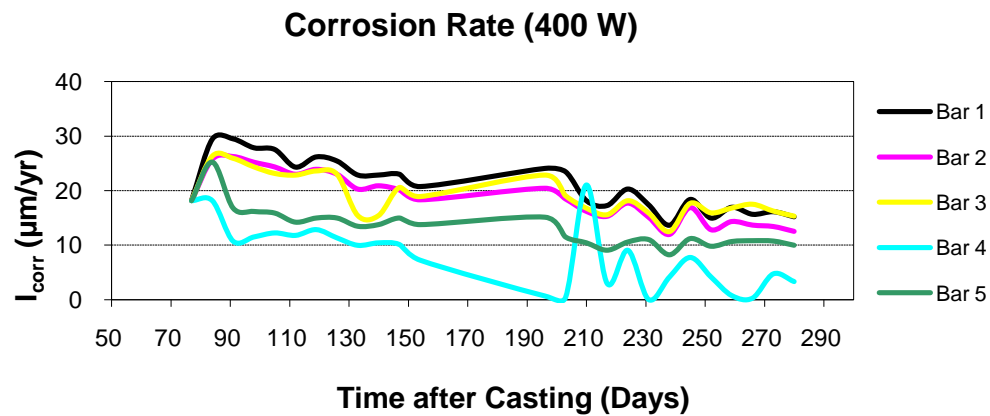


Figure 46: Macrocell corrosion current density for 400 W rebar in prisms

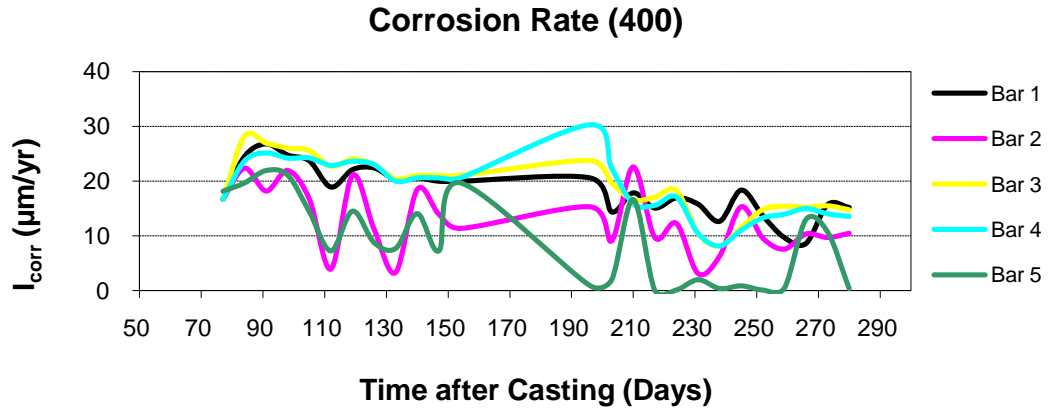


Figure 47: Macrocell corrosion current density for 400 rebar in prisms

4.2.ii Corrosion potential

The corrosion potential for the 316 LN bars in ASTM A 955M prisms started from at -200 to -300 mV SCE and went up to -100 mV SCE and for UNS 24100, 2304 and LDX 2101, the corrosion potential remained steady in the -200 mV to -100 mV SCE range, as shown below in Figure 48 to Figure 51.

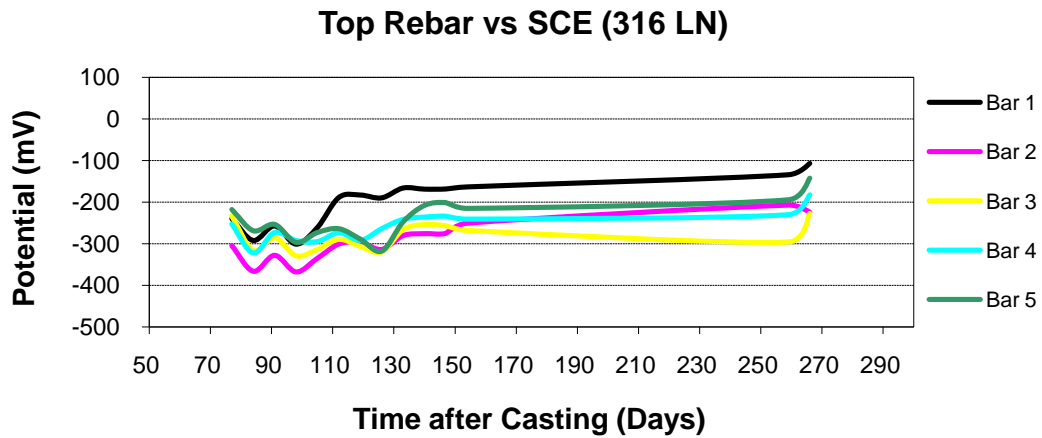


Figure 48: Corrosion potential for 316 LN top bars in prisms

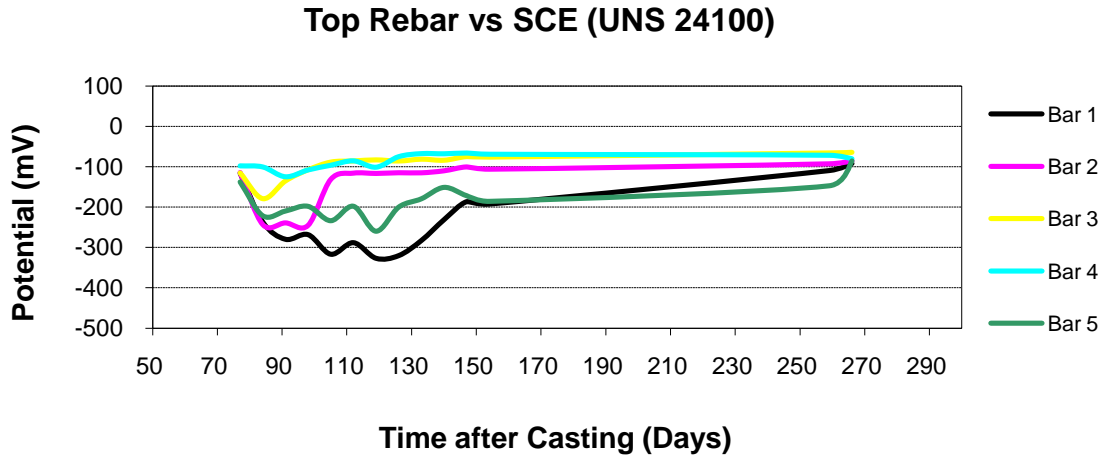


Figure 49: Corrosion potential for UNS 24100 top bars in prisms

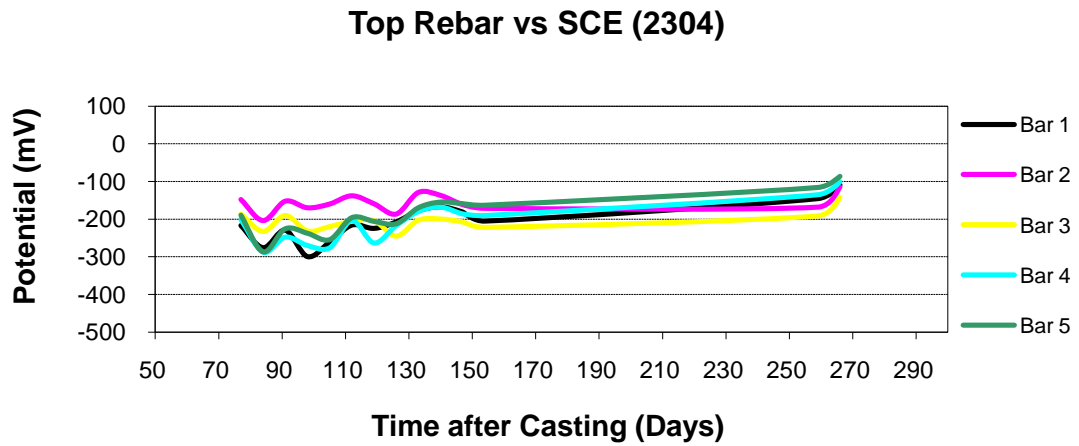


Figure 50: Corrosion potential for 2304 top bars in prisms

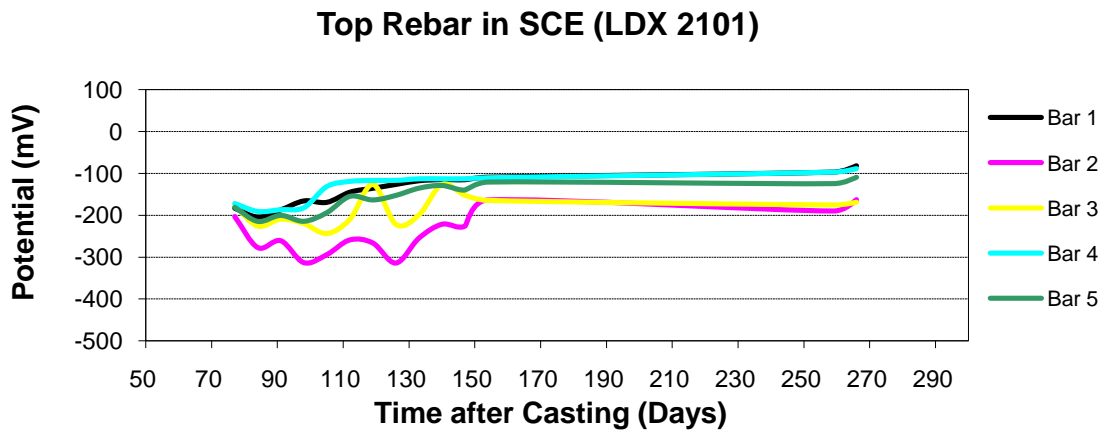


Figure 51: Corrosion potential for LDX 210 top bars in prisms

The corrosion potential for the 400 and 400 W bars in ASTM A 955M cracked prisms can be seen from the Figures 52 and 53 to be much more negative than in the accelerated test. It is clear that the chlorides penetrated the concrete through the crack immediately upon exposure of the specimens to the salt solution and these bars started corroding soon afterwards.

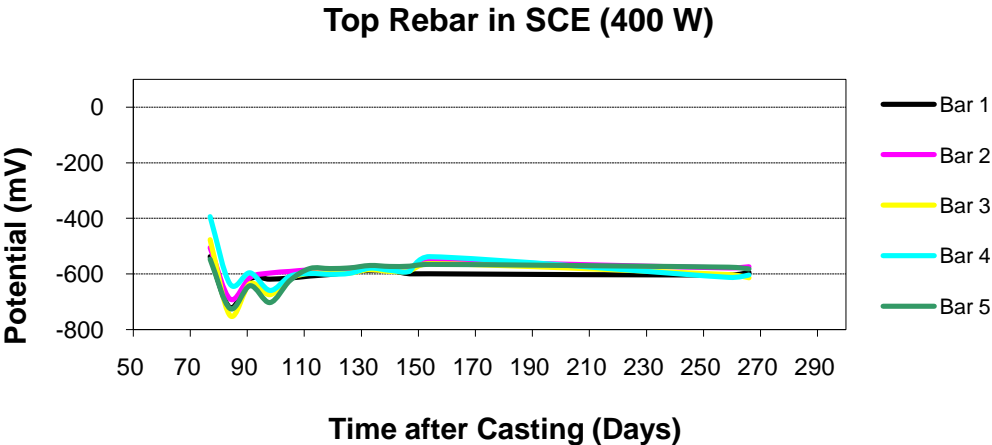


Figure 52: Corrosion potential for 400 W top bars in prisms

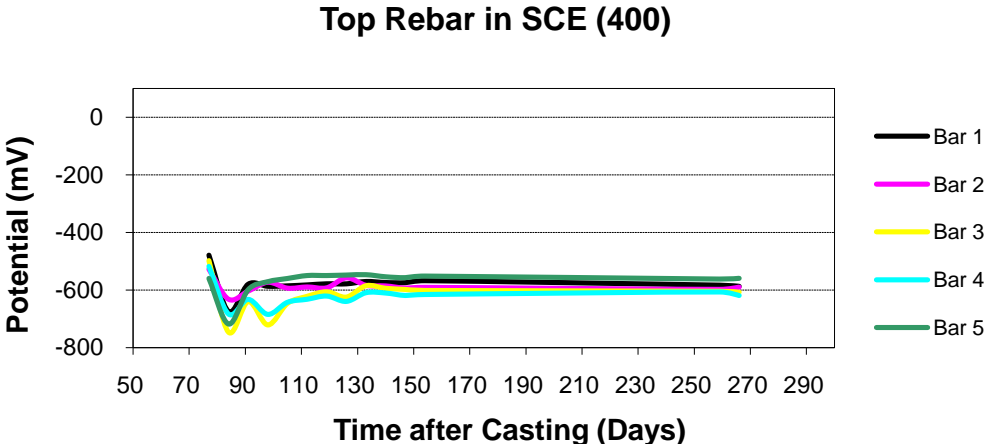


Figure 53: Corrosion potential for 400 top bars in prisms

The entire bottom rebar of the ASTM A 955M prisms show almost similar potentials as all of them are black steel and are all acting as cathodes in a macrocell. The little fluctuations are because of the voids and cracks in the beams for 400W prisms and bar no 4 for UNS 24100.

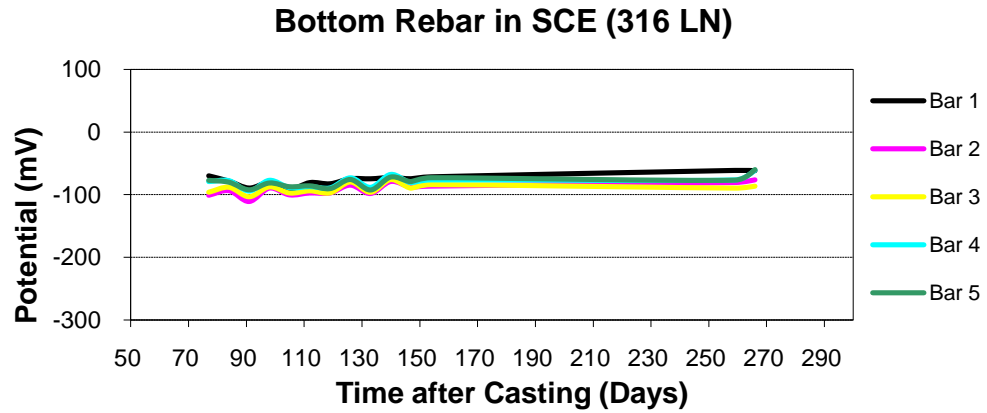


Figure 54: Corrosion potential for 316 LN bottom bars in prisms

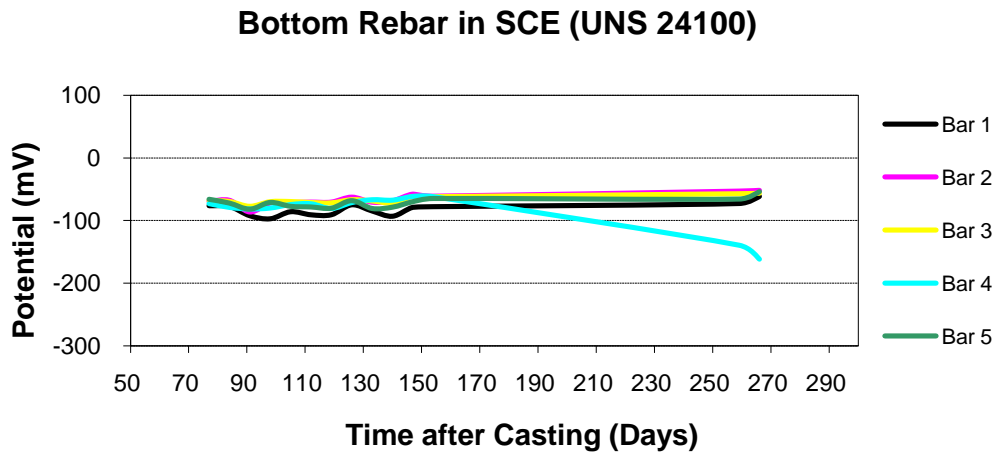


Figure 55: Corrosion potential for UNS 24100 bottom bars in prisms

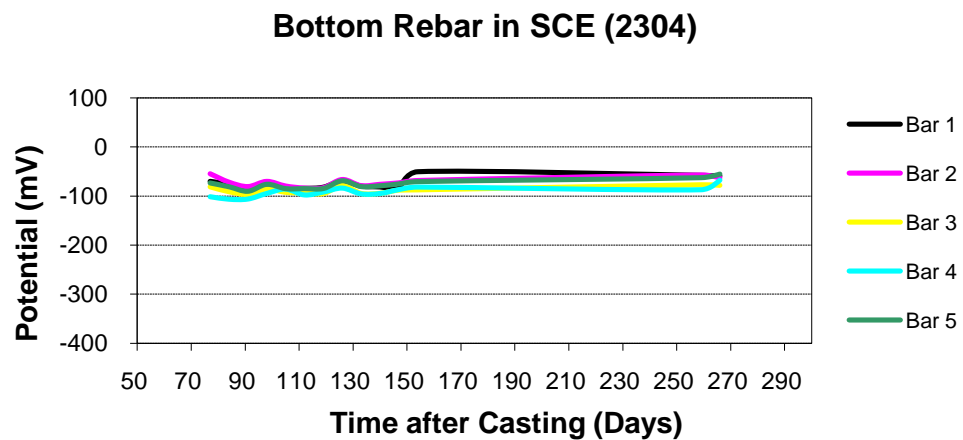


Figure 56: Corrosion potential for 2304 bottom bars in prisms

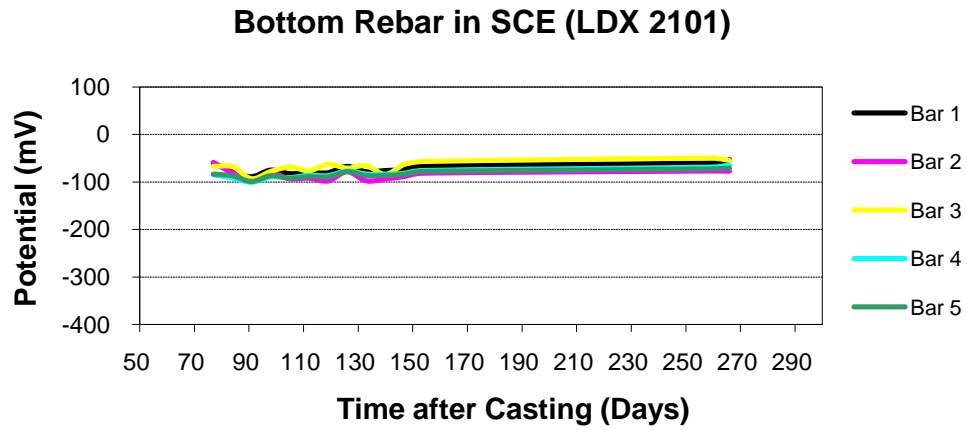


Figure 57: Corrosion potential for LDX 2101 bottom bars in prisms

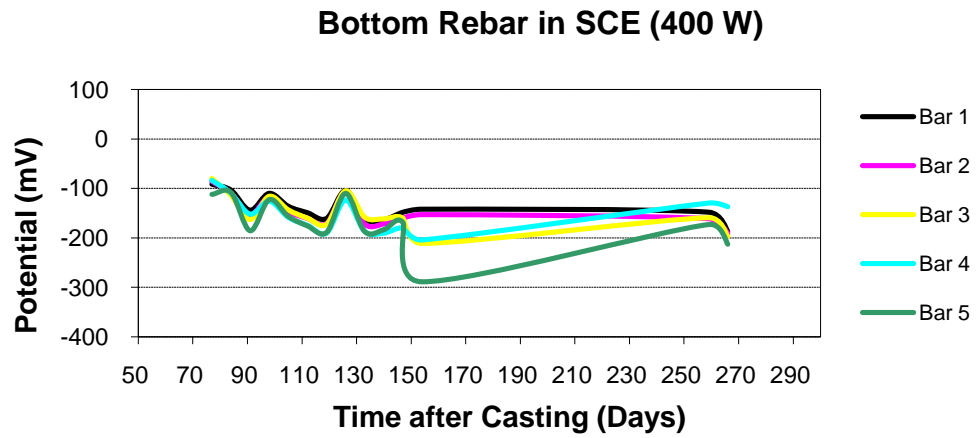


Figure 58: Corrosion potential for 400 W bottom bars in prisms

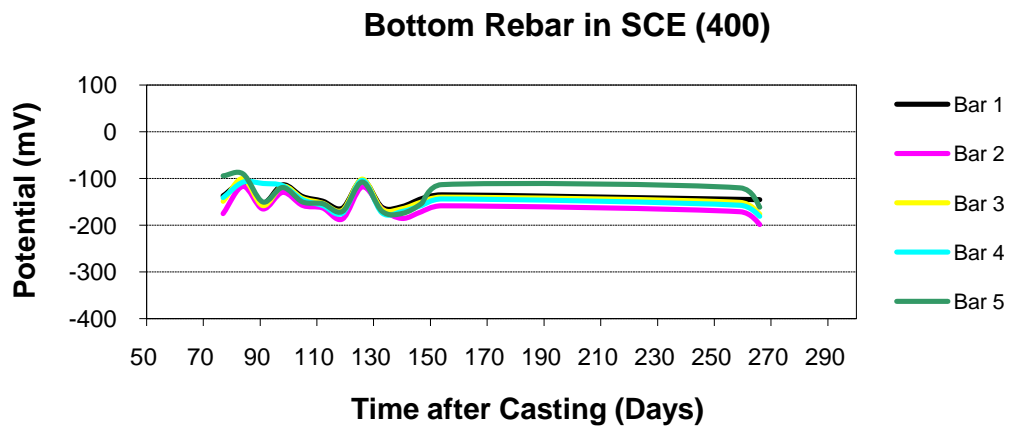


Figure 59: Corrosion potential for 400 bottom bars in prisms

4.2.iii Microstructure of the steels

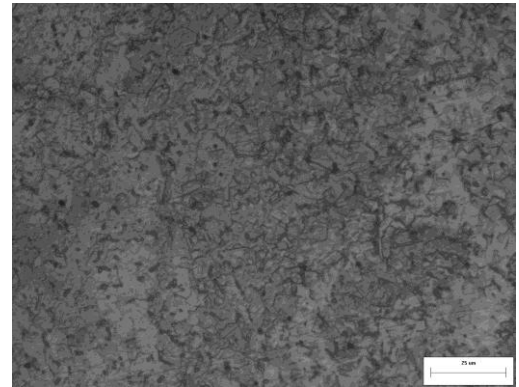
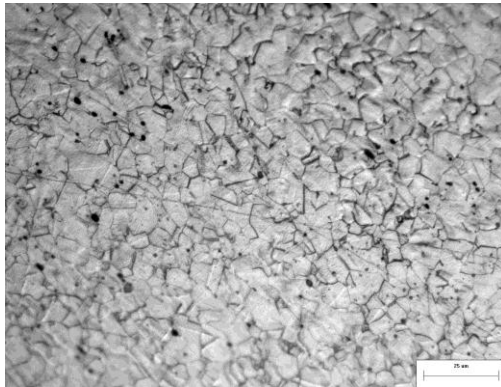


Figure 60: Microstructure of the 316 LN rebar Figure 61: Microstructure of the UNS 24100 rebar

The microstructure shows that 316 LN has the austenite phase and the grains are shown in the Figure 60, whereas, UNS 24100 has the ferrite phase and smaller grain sizes are shown in Figure 61 (Valbruna; M.F. Montemor et al., 1998).

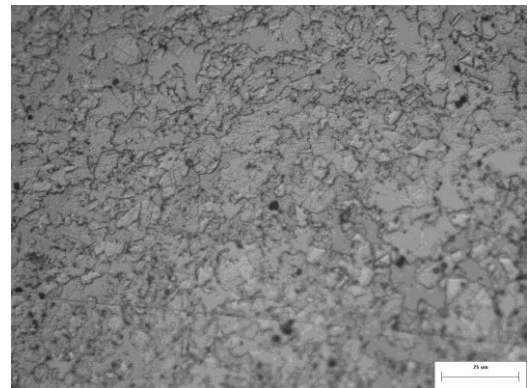
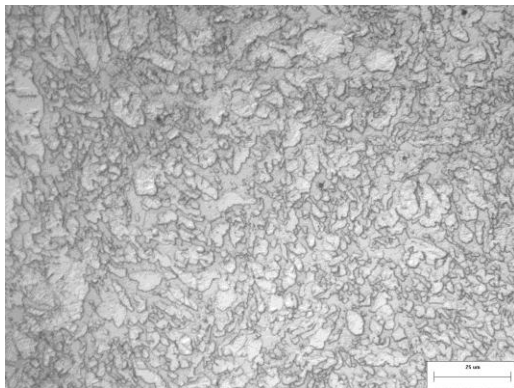


Figure 62: Microstructure of 2304 rebar Figure 63: Microstructure of LDX 2101 rebar

Duplex steel has the microstructure of both the ferritic and austenitic phases which can be seen from the microstructure of the 2304 and LDX 2101. LDX 2101 has the larger grain size than that of the 2304 stainless steel (Outokumpu; N. Alonso-Falleiros, 1999).

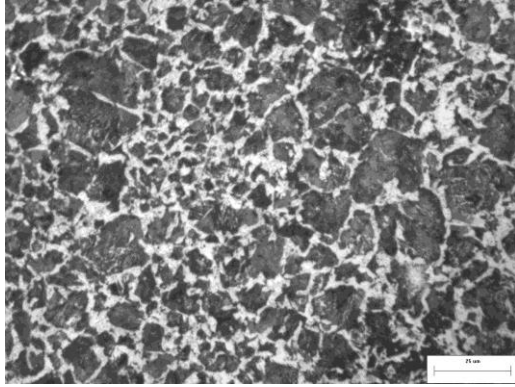


Figure 64: Microstructure of the 400 W rebar

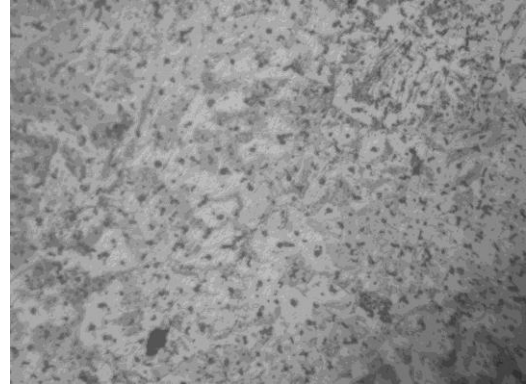


Figure 65: Microstructure of the 400 top and bottom rebar

The microstructure of the 400 W (Figure 63) have primary ferrite and pearlite having a larger grain size, in contrast 400 (Figure 64) which was used both as the top bar in one set of prisms and the bottom bars in all the prisms has smaller grain size.

4.2.iv Chloride analysis of the concrete of the beams

The chloride analysis of concrete was done after breaking open the three bars of the beams and grinding approximately 1-2 mm depth adjacent to the steel. The following procedure was followed during the titration procedure

- i) Initially AgNO_3 of 0.01M was used as the titrant to do the titration.
- ii) Then a solution of concrete was prepared according to the ASTM Standard C1152
- iii) After that the solution was titrated with a solution of 50 μl in 50 ml of water in Auto burette machine.
- iv) The data obtained in grams per litre of the 50 μl solution and then converted to weight percent of chloride in concrete

Chloride in concrete

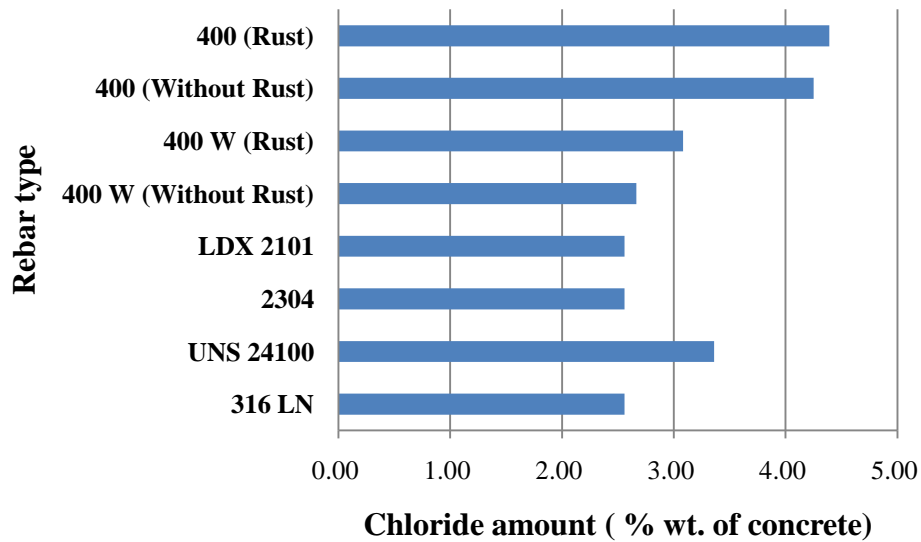


Figure 66: Weight percentage of chloride in concrete for the beams

The amount of chloride that penetrated in the concrete after 400 days of accelerated test is shown in the Figure 66 and was calculated on the basis of the weight percentage of chloride in concrete by titration procedure. It is found that the percentage of chloride for the 316 LN, 2304 & LDX 2101 beams was 2.56 and for UNS 24100 is 3.36 percent and no corrosion was found after breaking open. The higher chloride content value in the UNS 24100 is believed to be result of a few large voids in the concrete cover over the bars allowing greater ingress of the salt. Similar higher void content was observed in the cover concrete of the 400 black steel. Moreover, the percentage of chloride was found little bit higher where there were corrosion products for 400 and 400 W than the regions where there is no corrosion at all. The inspection of the rebar after autopsying revealed that the corrosion remained localised. The titration results indicate that, as the corroding areas become more anodic, the negative chloride ions are preferentially attracted to those areas.

5 Summary, Conclusions and Recommendations

Microcell corrosion test for 316 LN shows that corrosion potential for the accelerated testing increased from -100 mV to -300 mV and the corrosion current density remained up to 0.3 mA^2 ($0.348 \text{ } \mu\text{m}/\text{yr}$). However, for the same bars in cracked ASTM A 955M sample showed that corrosion potential remains almost the same and current density around $0.1 \text{ } \mu\text{m}$ per year. Though these data were taken only for 400 and 200 days, further data should be taken for future study as stainless steel do not show any sign of corrosion. Moreover, the amount of chloride penetrated in the accelerated testing does not result in corrosion on 316 LN easily.

During the accelerated corrosion testing in beams for UNS 24100, the corrosion potential and the corrosion current density remains steady; whereas, during the cracked prisms test the corrosion potential was more negative and corrosion current density almost steady and the test should continue to give better understanding of the corrosion phenomenon of these stainless steel bars.

Duplex steel like 2304 showed steady change in potential and corrosion current density both in accelerated and ASTM A 955M cracked environment. The macrocell current density fluctuated after few weeks as the salt penetrated through the cracked concrete faster. LDX 2101 is duplex steel that was used to compare with the 316 LN stainless steel and showed steady values in both corrosion potential and current density in accelerated and ASTM A 955M tests.

Weldable black steel (400 W) still showed initiation of corrosion both in accelerated and macrocell tests and after the initiation of corrosion all the corrosion potential and current density remained steady.

Regular black steel (400) has shown more negative potential in ASTM 955 prisms than in accelerated corrosion testing as the chloride was going directly on the surface. The corrosion current densities for accelerated testing become steady after the initiation of

corrosion and, for the cracked prisms, it started to drop after certain period. It is due to the formation of the rusts on the surface of the black steels which were found after cracking the beams as the prisms have more negative corrosion potential than beams.

References

- Aal, E.E. Abd El, S. Abd El Wanees, A. Diab, S.M. Abd El Haleem. "Environmental factors affecting the corrosion behavior of reinforcing steel III. Measurement of pitting corrosion currents of steel in Ca(OH)₂ solutions under natural corrosion conditions." *Corrosion Science* 51 (2009): 1611-1618.
- Ahmad, Shamsad. "Reinforcement corrosion in concrete structures, its monitoring and service life prediction—a review." *Cement & Concrete Composites* 25 (2003): 459–471.
- Alonso, M. C. and M. Sanchez. "Analysis of the variability of chloride threshold values in the literature." *Materials and Corrosion* 60, no. 08 (2009): 631-637.
- Alonsoa, C., C. Andradea, M. Castellotea, P. Castro. "Chloride threshold values to depassivate reinforcing bars embedded in a standardized OPC mortar." *Cement and Concrete Research* 30 (2000): 1047-1055.
- Alonso-Falleiros, N., A. Hakim and S. Wolyneec. "Comparison between potentiodynamic and potentiostatic tests on the pitting corrosion measurement of the duplex stainless steel." 55, no. 5 (May 1999): 443-448.
- Andrade, C., I. R. Maribona, S. Feliu, J. A. Gonzalez and S. Feliu jr., "The effect of the marocells between active and passive areas of the steel reinforcement." *Corrosion Science* 33, no. 2 (1992): 231-249.
- Angst, Ueli, Bernhard Elsener, Claus K. Larsen, Øystein Vennesland. "Critical chloride content in reinforced concrete — A review." *Cement and Concrete Research* 39 (2009): 1122-1138.
- Ann, K.Y., J.H. Ahn, J.S. Ryou. "The importance of chloride content at the concrete surface in assessing the time to corrosion of steel in concrete structures." *Construction and Building Materials* 23 (2009): 239-245.
- ASTM - A 615. *Standard specification for deformed and plain stainless-steel bars for concrete reinforcement*. West Conshohocken, Pennsylvania 19428-2959, United States: ASTM International, 2007.
- ASTM A 955/A 955M-07a. *Standard specification for deformed and plain stainless-steel bars for concrete reinforcement*. West Conshohocken, Pennsylvania 19428-2959, United States: ASTM International, 2007.

ASTM C 876-09. *Standard test method for corrosion potentials of uncoated reinforcing steel in concrete*. West Conshohocken, Pennsylvania 19428-2959: ASTM International, 2009.

ASTM G 1-03. *Standard practice for preparing, cleaning, and evaluating corrosion test specimen*. West Conshohocken, Pennsylvania 19428-2959, United States: ASTM International, 2003.

ASTM G 109-07. *Standard test method for determining effects of chemical admixtures on corrosion of embedded steel reinforcement in concrete exposed to chloride environments*. West Conshohocken, Pennsylvania 19428-2959, United States: ASTM International, 2007.

ASTM G 3-89. *Standard practice for conventions applicable to corrosion measurements in corrosion testing*. West Conshohocken, Pennsylvania 19428-2959, United States: ASTM International, 2004.

ASTM G 44-99. *Standard practice for exposure of metals and alloys by alternate immersion in neutral 3.5 % sodium chloride solution*. West Conshohocken, Pennsylvania 19428-2959, United States: ASTM International, 2005.

Beck, M., J. Goebbels, A. Burkert, B. Isecke and R. Bassler. "Monitoring of corrosion processes in chloride contaminated mortar by electrochemical measurements and X-ray tomography." *Materials and Corrosion* 60, no. 9999.

Berke, N.S., M.P. Dallaire, M.C. Hicks, and R.J. Hoopes. "Corrosion of Steel in Cracked Concrete." 49, no. 11 (November 1993): 934-943.

Bertolini, L., E.Redaeli. "Depassivation of steel reinforcement in case of pitting corrosion: detection techniques for laboratory studies." *Materials and Corrosion* 60, no. 08 (2009): 608-616.

Bertolini, L., F. Bolzonio, M. Gastaldi, T. Pastoreb, P. Pedferri, E. Redaeli. "Effects of cathodic prevention on the chloride threshold for steel corrosion in concrete." *Electrochimica Acta* 54 (2009): 1452-1463.

Bertolini, Luca, Maddalena Carsana, Pietro Pedferri. "Corrosion behavior of steel in concrete in the presence of stray current." *Corrosion Science* 49 (2007): 1056 – 1068.

Bonen, David. "A micro structural study of the effect produced by the magnesium on plain and silica fume bearing Portland mortars." *Cement and Concrete research* 23 (1993): 541-553.

Buenfield, N. R. and G. K. Glass. "The presentation of the chloride threshold level for corrosion of steel in concrete." *Corrosion Science* 39, no. 05 (1997): 1001-1013.

Burstein, G.T., P.C. Pistorius. "Surface roughness and the metastable pitting of stainless steel in chloride solutions." *Corrosion* 51, no. 5 (1995).

Cairns, J., Y. Du, D. Law. "Influence of corrosion on the friction characteristics of the steel/concrete interface." *Construction and Building Materials* 21 (2007): 190–197.

Chen, D. and Sankaran Mahadevan. "Chloride-induced reinforcement corrosion and concrete cracking simulation." *Cement & Concrete Composites* 30 (2008): 227–238.

El Maaddawy, Tamer and Khaled Soudki. "A model for prediction of time from corrosion initiation to corrosion cracking." *Cement & Concrete Composites* 29 (2007): 168–175.

Elsener, B. "Corrosion rate of steel in concrete—Measurements beyond the Tafel law." *Corrosion Science* 47 (2005): 3019–3033.

Elsener, B., L. Zimmermann, H. Bohni. "Non destructive determination of the free chloride content in cement based materials." *Materials and Corrosion* 54 (2003): 440-446.

Fanga, Conqi, Karin Lundgrenb, Liuguo Chena, Chaoying Zhu. "Corrosion influence on bond in reinforced concrete." *Cement and Concrete Research* 34 (2004): 2159–2167.

Feliu, S., J. A. Gonzalez, J. M. Miranda, V. Feliu. "Possibilities and problems of in situ techniques for measuring steel corrosion rates in large reinforced concrete structures." *Corrosion Science* 47 (2005): 217–238.

Frederiksen, J. M. "On the need for more precise threshold values for chloride initiated corrosion." *Materials and Corrosion* 60, no. 08 (2009): 597-601.

Fu, Yan, Jian Ding, J.J. Beadoin. "Expansion of portland cement mortar due to the internal sulfate attack." *Cement and Concrete research* 27, no. 9 (1997): 1299-1306.

Gonzalez, J.A., C. Andrade, C. Alonso and S. Feliu. "Comparison of rates of general corrosion and maximum pitting penetration on concrete embedded steel reinforcement." *Cement and Concrete Research* 25, no. 02 (1995): 257-264.

González, J.A., J.M. Miranda, N. Birbilis, and S. Feliu. "Electrochemical techniques for Studying Corrosion of Reinforcing Steel: Limitations and Advantages." 61, no. 01 (January 2005): 37-50.

González, J.A., S. Feliu, and P. Rodríguez. "Threshold steel corrosion rates for durability problems in reinforced structures." *Corrosion* 53, no. 01 (1997): 65-71.

Hansson, C.M. "Comments on electrochemical measurements of the rate of corrosion of steel in concrete." *Cement and Concrete Research* 14 (1984): 574-584.

Hansson, C.M. "Concrete: The advance industrial material of the 21st century." *Metallurgical and Materials Transactions A* 26A (1995): 1321-1341.

Hansson, C.M., A. Poursaei, A. Laurent. "Macrocell and microcell corrosion of steel in ordinary portland cement and high performance concretes." *Cement and Concrete Research* 36 (2006): 2098–2102.

Hansson, C.M., Th. Fr. lund and J. B. Markussen. "The effect of chloride cation type on the corrosion of steel in concrete by chloride salts." *Cement and Concrete Research* 15 (1985): 65-73.

Hassan, A.A.A., K.M.A. Hossain, M. Lachemi. "Corrosion resistance of self-consolidating concrete in full-scale reinforced beams." *Cement & Concrete Composites* 31 (2009): 29-38.

Hausmann, D. A. *Material Properties* 6 (1967): 19.

Hime, William G. and Bryant Mather. "Sulfate attack or is it." *Cement and Concrete research* 29 (1999): 789 - 791.

Hope, Brian B., Alan K. Ip. "Corrosion and electrical impedance in concrete." *Cement and Concrete Research* 15 (1985): 525-534.

Hope, Brian B., John A. Page and Alan K.C. Ip,. "Corrosion rates of steel in concrete." *Cement and Concrete Research* 16 (1986): 771-781.

Idrissia, H., A. Limam. "Study and characterization by acoustic emission and electrochemical measurements of concrete deterioration caused by reinforcement steel corrosion." *NDT & E International* 36 (2003): 563–569.

Ismail, M., A. Toumi, R. François, R. Gagné. "Effect of crack opening on the local diffusion of chloride in cracked mortar samples." *Cement and Concrete Research* 38 (2008): 1106-1111.

Koichi, Kobayashi. "A study of the electrochemical properties of the stainless steel rebar used patching for chloride induced corrosion RC member." *Japan Society of Material Science* 54, no. 06 (June 2005): 636-641.

Li, L., A.A. Sagiés. "Chloride corrosion threshold of reinforcing steel in alkaline solutions—open-circuit immersion tests." *Corrosion* 57, no. 01 (January 2001): 19-28.

Lawrance, C. D. "The influence of binder type on sulfate." *Cement and Concrete research* 22 (1992): 1047 -1058.

Lee, Han-Seung and Young-Sang Cho. "Evaluation of the mechanical properties of steel reinforcement embedded in concrete specimen as a function of the degree of reinforcement corrosion." *Int J Fract* 157 (2009): 81-88.

Li, Chun-Qing, Yang Yang, and Robert E. Melchers. "Prediction of reinforcement corrosion in concrete and its effects on concrete cracking and strength reduction." *ACI Materials Journal* 105, no. 01 (January-February 2008).

Li, Lianfang and Alberto A. Sagues. "Metallurgical effects on chloride ion corrosion threshold of steel in concrete." Final report to the Florida Department of Transportation, of Civil and Environmental Engineering, University of South Florida, 2001.

Lundgren, K. "Effect of corrosion on the bond between steel and concrete: an overview." *Magazine of Concrete Research* 59, no. 06 (2007): 447–461.

Mammoliti, L. L., L.C. Brown, C. M. Hansson and B. B. Hope. "The influence of the surface finish of reinforcing steel and pH of the test solution on the chloride threshold concentration for corrosion initiation in synthetic pore solution." *Cement and Concrete Research* 26, no. 04 (1996): 545-550.

Mansfeld, F. "Discussion: Electrochemical Techniques for Studying Corrosion of Reinforcing Steel: Limitations and Advantages." *Corrosion* 61, no. 08 (August 2005): 739-742.

Martínez, I., C. Andrade. "Application of EIS to cathodically protected steel: Tests in sodium chloride solution and in chloride contaminated concrete." *Corrosion Science* 50 (2008): 2948–2958.

Mehta, P. K. *Concrete structure, properties, and materials*. Prentice-Hall International, 1986.

Melchers, R.E. "Effect of Temperature on the Marine Immersion Effect of Temperature on the Marine Immersion." *Corrosion* 58, no. 09 (September 2002): 768-782.

Mohammed, T. U. and H. Hamada. "Corrosion of Steel Bars in Concrete with Various Steel Surface Conditions." *ACI Materials Journal* 103, no. 04 (July-August 2006): 233-242.

Moreno, M., W. Morris, M.G. Alvarez, G.S. Duffo. "Corrosion of reinforcing steel in simulated concrete pore solutions effect of carbonation and chloride content." *Cement and Concrete Research* 46 (2004): 2681–2699.

Morris, W., A. Vico, M. Vázquez. "Chloride induced corrosion of reinforcing steel evaluated by concrete resistivity measurements." *Electrochimica Acta* 49 (2004): 4447–4453.

Naqvia, A.A., M.M. Nagadia, O.S.B. Al-Amoudi. "Prompt gamma analysis of chlorine in concrete for corrosion study." *Applied Radiation and Isotopes* 64 (2006): 283-289.

Nehdi, M. and M. Hayek. "Behavior of blended cement mortar exposed to sulfate solutions cycling in relative humidity." *Cement and concrete research* 35 (2005): 731-742.

Newman, R.C. "2001 W.R. Whitney Award Lecture: Understanding the Corrosion of Stainless Steel." *Corrosion* 57, no. 12 (December 2001): 1030-1041.

Oh, B. H., S. Y. Jang and Y. S. Shin. "Experimental investigation of the threshold chloride concentration for corrosion initiation in reinforced concrete structures." *Magazine of Concrete Research* 55, no. 02 (April 2003): 117-124.

Rodríguez, P., E. Ramírez, S. Feliu, J.A. González, and W. López. "Significance of coplanar macrocells to corrosion in concrete-embedded steel." *Corrosion* 55, no. 03 (March 1999): 319-325.

Venkatesan, P.,N. Palaniswamy, K. Rajagopal. "Corrosion performance of coated reinforcing bars embedded in concrete and exposed to natural marine environment." *Progress in Organic Coatings* 56 (2006): 8–12.

Page, C. L. "Initiation of chloride-induced corrosion of steel in concrete: role of the interfacial zone." *Materials and Corrosion* 60, no. 08 (2009): 586-592.

Poupard, O., V. L'Hostis, S. Catinaud, I. Petre-Lazar. "Corrosion damage diagnosis of a reinforced concrete beam after 40 years natural exposure in marine environment." *Cement and Concrete Research* 36 (2006): 504 – 520.

Pourbaix, Marcel. "*Atlas of electrochemical equilibria in aqueous solutions.*" Second English Edition, NACE, 1974.

Poursae, A. and C.M Hansson. "Potential pitfalls in assessing chloride-induced corrosion of steel in concrete." *Cement and Concrete Research* 39 (2009): 391 - 400.

Pradhan, Bulu and B. Bhattacharjee. "Half-Cell potential as an indicator of chloride-induced rebar corrosion initiation in RC." *Journal of Materials in Civil Engineering* 21, no. 10 (October 2009): 543-554.

RILEM. "Draft recommendation for the repair strategies for concrete structures damaged by the reinforcement corrosion." *Materials and structure*, 1994: 415 - 436.

Rodríguez, P., E. Ramírez, S. Feliu, J.A. González, and W. López. "Significance of coplanar macrocells to corrosion in concrete-embedded steel." *Corrosion* 55, no. 03 (1999): 319-325.

Rodriguez, P., Ramirez E, Gonzalez JA. "Methods for studying corrosion in the reinforced concrete." *Magazine Concrete Research* 46, no. 167 (1994): 81-90.

Rong-Gui Du, Rong-Gang Hu, Ruo-Shuang Huang, and Chang-Jian Lin. "In Situ Measurement of Cl⁻ Concentrations and pH at the Reinforcing Steel/Concrete Interface by Combination Sensors." *Analytical Chemistry* 78, no. 09 (May 2006): 3179-3185.

Ryan, Mary P., David E. Williams, Richard J. Chater, Bernie M. Hutton. "Why stainless steel corrodes." *Nature* 415 (2002): 770-774.

Silverman, D. C. "Tutorial on cyclic polarization technique." NACE, 1998: 1-21.

Song, Ha-Won and Velu Saraswathy. "Corrosion monitoring of reinforced concrete structures - A review." *International Journal of Electrochemical Science* 02 (2007): 1-28.

Trejo, David, Radhkrisna G. Pillai. "Accelerated chloride threshold testing: Part I - ASTM A 615 and A 706 Reinforcement." *ACI Materials Journal* 100, no. 06 (November-December 2003): 519-527.

Trejoa, David, Paulo J. Monteiro. "Corrosion performance of conventional (ASTM A615) and low-alloy (ASTM A706) reinforcing bars embedded in concrete and exposed to chloride environments." 35 (2005): 562–571.

Wang, S. and R.C. Newman. "Crevice corrosion of type 316L Stainless Steel in alkaline chloride solutions." *Corrosion* 60, no. 05 (May 2004): 448-454.

Yunovich, Mark, Neil G. Thompson, Tunde Balvanyos, Lester Lave. "Highway bridges." 2001.

Zhang, J., Noël P. Mailvaganam. "Corrosion of concrete reinforcement and electrochemical factors in concrete patch repair." *Canadian Journal of Civil Engineering* 33 (2006): 785–793.

Appendix A

Drill bits and Taps

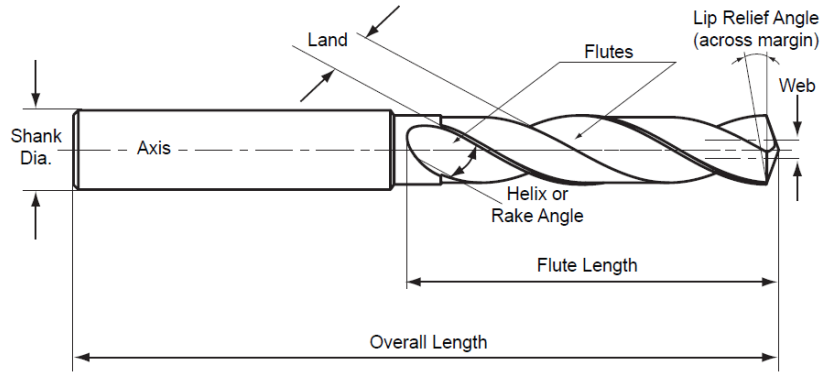


Figure 67: Drill terminology

The picture shows the drill terminology of all drills in common. The drill bit used was the spiral drill bit made from carbide materials and taps used made from high speed steel.

Appendix B

Reference Electrodes

There are several different types of electrodes present. The reference electrode used for the accelerated corrosion testing of the beams was Mn/MnO₂ electrode supplied by Force Technology. These electrodes were embedded inside the concrete during the casting of the concrete. The electrode consists of a steel housing with an alkaline chloride free gel having pH equal to 13.5. The front part, porous plug, is made with cement based materials with fibre reinforcement.

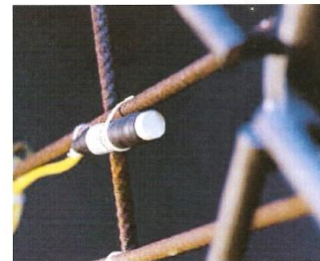
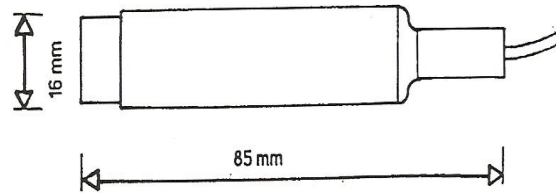


Figure 68: Schematic diagram and actual picture of the reference electrode

The following table shows the reference electrodes data with reference to saturated calomel electrode (SCE)

Beams	ERE 20 No	Supplier's Data	Lab Data
		mV vs SCE	mV vs SCE
UNS 24100	R 14774	182	139
316 LN	R 14769	181	156
2304	R 14770	180	142
LDX 2101	R 14772	186	157
400 W	R 14767	186.2	135
400	R 14768	170	143

Table 7 : Reference electrode potential with respect to SCE

The typical value for Mn/MnO₂ reference electrode in Ca(OH)₂ at 23° C is +200 mV with respect to SCE. The potentials for all the Mn/MnO₂ reference electrode normally lies in between +170mV to + 220 mV with respect to SCE. For the cracked G 109 prisms, saturated calomel electrode (SCE) was used as a reference electrode.

Appendix C

Titanium Mesh

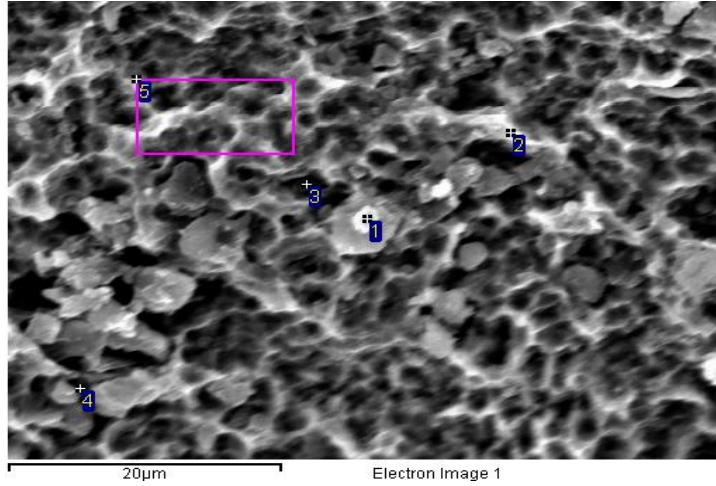


Figure 69: SEM picture for Titanium mesh (250X) for EDS analysis

All results in weight% Processing option: All elements analysed (Normalised)

Spectrum	In stats.	Ti	Ir	Pt	Au	Total
1	Yes	90.60	0.85	0.34	8.21	100.00
2	Yes	82.22	4.14	0.52	13.13	100.00
3	Yes	75.04	5.48	3.01	16.48	100.00
Mean		82.62	3.49	1.29	12.61	100.00
Std. deviation		7.79	2.38	1.49	4.16	
Max.		90.60	5.48	3.01	16.48	
Min.		75.04	0.85	0.34	8.21	

Table 8 : EDS data after the analysis of the Titanium mesh

Appendix D
Concrete Composition

CSA Class F-1 concretes	Beams	G109 Prisms
Gravel 20 mm	3180 kg
Gravel 14 mm	1575 kg
Sand	2590 kg	1330 kg
General use cement	798 kg	403 kg
Slag	144 kg	79 kg
Euclid AirEx-L	332 ml
Euclid AirExtra	210 ml
Euclid Water Reducer	2369 ml	1265 ml
Water	250 l	117 l
Moisture in sand	85 l	52 l

Table 9 : Concrete composition for beams and prisms

Appendix E

Actual Composition of the Rebar

Alloy	C	N	Cr	Ni	Mo	Mn	P	S	Si
316LN	0.02	0.10	18.1	10.9	2.07	1.13	0.031	0.019	0.64
UNS 24100	0.06	0.282	17.3	0.68	0.14	11.6	0.026	0.056	<0.01
2304	0.04	0.130	22.7	3.8	0.27	1.52	0.029	<0.005	0.54
LDX 2101	0.04	0.230	21.1	1.20	0.17	5.10	0.023	<0.005	0.74
400 W	0.37	0.016	0.11	0.16	0.04	0.77	0.012	0.037	0.19
400 - T	0.28	0.010	0.19	0.17	0.05	1.26	0.024	0.027	0.19
400 - B	0.22	0.010	0.06	0.05	<0.01	1.88	0.016	0.021	0.33

Alloy	V	Ti	Nb	Al	Cu
316LN	0.064	<0.005	0.018	0.01	0.59
UNS 24100	<0.005	<0.005	0.013	0.01	0.18
2304	0.084	<0.005	0.012	0.01	0.32
LDX 2101	0.112	<0.005	0.008	0.01	0.34
400 W	<0.005	<0.005	0.014	<0.005	0.32
400 - T	0.048	0.14	<0.005	<0.005	0.37
400 - B	0.048	<0.005	<0.005	<0.005	0.23

Table 10 : Actual composition of the rebar (weight percent) after analysis